AFOSR-TR- 79-1319

LEVEL II

AO79658

8

SC

AD A079659

DDC FILE COPY

DDC
RECEIVED
JAN 21 1980
D

Approved for public release;
distribution unlimited.

80 1 16 083

UNCLASSIFIED

SECURITY CLASSIFICATION OF THIS PAGE (When Data Entered)

REPORT DOCUMENTATION PAGE	READ INSTRUCTIONS BEFORE COMPLETING FORM
1. REPORT NUMBER: AFOSR-TR-79-1319	2. GOVT ACCESSION NO. / 3. RECIPIENT'S CATALOG NUMBER
4. TITLE (and Subtitle): CRUSTAL AND UPPER MANTLE VELOCITY & Q STRUCTURES OF MAINLAND CHINA	5. TYPE OF REPORT & PERIOD COVERED: Interim
	6. PERFORMING ORG. REPORT NUMBER
7. AUTHOR(s): Ta-liang Teng	8. CONTRACT OR GRANT NUMBER(s): F49620-76-C-0010, ARPA Order-3291
9. PERFORMING ORGANIZATION NAME AND ADDRESS: Geophysical Laboratory, University of Southern California, Los Angeles, CA 90007	10. PROGRAM ELEMENT, PROJECT, TASK AREA & WORK UNIT NUMBERS: 62701E 9F10, A.O.3291-21
11. CONTROLLING OFFICE NAME AND ADDRESS: DARPA/NMR, 1400 Wilson Blvd., Arlington, VA 22209	12. REPORT DATE: November 1979 / 13. NUMBER OF PAGES: 66
14. MONITORING AGENCY NAME & ADDRESS(if different from Controlling Office): AFOSR/NP, Bolling AFB, Bldg.#410, Wash DC 20332	15. SECURITY CLASS. (of this report): unclassified / 15a. DECLASSIFICATION/DOWNGRADING SCHEDULE
16. DISTRIBUTION STATEMENT (of this Report): Approved for public release; distribution unlimited.	
17. DISTRIBUTION STATEMENT (of the abstract entered in Block 20, if different from Report): Semi-annual technical rept.	
18. SUPPLEMENTARY NOTES	
19. KEY WORDS (Continue on reverse side if necessary and identify by block number): 408856	

20. ABSTRACT (Continue on reverse side if necessary and identify by block number)

Repeated surface wave group velocity measurements over the same paths were made by using large aftershocks of several great (M greater than 7) earthquakes recently occurred in China. Multiple filter technique was applied to the properly rotated three-component digital data from Seismolcgical Research Observatory (SRO) stations, so that both Rayleigh- and Love-wave dispersion data were obtained over a number of paths crossing various tectonic provinces of China. In several cases, higher mode data were also derived. An estimate of uncertainty of these dispersion data was obtained from the repeated measurements

DD FORM 1 JAN 73 1473 EDITION OF 1 NOV 65 IS OBSOLETE

UNCLASSIFIED

with identical source-receiver geometry. The generalized surface wave inversion technique was applied to these multi-mode dispersion data, and crustal and upper mantle structures were derived for various tectonic provinces of China. The results clearly demonstrate that the Chinese Mainland is far from being laterally homogeneous, the lateral heterogeneities closely reflect the tectonic developments in the recent past. A particularly unusual crustal and upper mantle structure is found underlying the Tibet plateau.

LEVEL I

SEMI-ANNUAL TECHNICAL REPORT

submitted to the

AIR FORCE OFFICE OF SCIENTIFIC RESEARCH

by the

GEOPHYSICAL LABORATORY
UNIVERSITY OF SOUTHERN CALIFORNIA

Contractor:	University of Southern California
Effective Date of Contract:	July 2, 1976
Expiration Date of Contract:	October 31, 1979
Amount of Contract:	$143,003.00
Contract Number:	F49620-76-C-0010
Principal Investigator:	Ta-liang Teng (213) 741-6124
Program Manager:	Bill Best Bolling Air Force Base
Title:	CRUSTAL AND UPPER MANTLE VELOCITY & Q STRUCTURES OF MAINLAND CHINA
Sponsored by:	Advanced Research Projects Agency (DOD) ARPA Order No. 3291 Monitored by AFOSR

ABSTRACT

Repeated surface wave group velocity measurements over the same paths were made by using large aftershocks of several great (M > 7) earthquakes recently occurred in China. Multiple filter technique was applied to the properly rotated three-component digital data from Seismological Research Observatory (SRO) stations, so that both Rayleigh- and Love-wave dispersion data were obtained over a number of paths crossing various tectonic provinces of China. In several cases, higher mode data were also derived. An estimate of uncertainty of these dispersion data was obtained from the repeated measurements with identical source-receiver geometry. The generalized surface wave inversion technique was applied to these multi-mode dispersion data, and crustal and upper mantle structures were derived for various tectonic provinces of China. The results clearly demonstrate that the Chinese Mainland is far from being laterally homogeneous, the lateral heterogeneities closely reflect the tectonic developments in the recent past. A particularly unusual crustal and upper mantle structure is found underlying the Tibet plateau.

INTRODUCTION

China has been divided tectonically into four major subplates by Sun and Teng (1977) based on surface geology. These subplates include (Figure 1):

(1) Chinghai-Tibet (southwestern China),

(2) North China,

(3) South China, and

(4) Northwestern China (including the Tien Shan fold belt).

These subdivisions are similar to those of McElhinny (1973), based on paleomagnetic data; Whittington and Hughes (1972) and Jell (1973), based on paleontologic data; and Dewey and Bird (1970), Hamilton (1970) and Burrett (1974), based on regional geology. Each subplate has different geomorphologic features, gravity anomalies and crustal thickness (Tung, 1974; Sun and Teng, 1977). A generalized compilation of the results of seismic reflection and refraction as well as gravity surveys has resulted in the inferred crustal thickness contours shown in Figure 1 (Chinese Academy of Sciences, 1974). Major seismic events occur along the subplate boundaries. This seismicity is related to the large-scale tectonic movements discussed by Molnar and Tapponier (1975, 1977).

The division of China into four major subplates is helpful from the standpoint of surface wave dispersion studies. The concept of regionalization, first proposed by Töksoz and Anderson (1966), consists of dividing a surface wave path into oceanic, shield and mountain tectonic regions. Each region has a different effect upon the average group velocity. Töksoz and Anderson (1966) noted that shield areas raise the average group velocity, whereas active tectonic regions have the effect of lowering the average group velocity. As a result, surface wave paths crossing different tectonic regions should show different trends in their average group velocity dispersion curves. The relationship between the concept of regionalization and its tectonic implications has been studied (Tung, 1974); the results show that it is appropriate to

divide China tectonically into several subplates, so that relatively pure path surface wave dispersion data can be derived for crustal and upper mantle structure inversion. This paper makes use of the digital data that has become available from numerous large aftershocks due to the recent occurrences of several large events (M > 7) inside China, and extracts dispersion information for a detailed analysis on the crustal and upper mantle structures.

Tectonic Setting of China

The tectonic setting of the four subplates of China proposed by Sun and Teng (1977) are:

1) The Chinghai-Tibet subplate consists of the area north of the Himalayas including the Kun Lun Mountains. Its eastern boundary coincides with the western border of Szechwan and Yunnan provinces at approximately longitude 105° E. Its western boundary is less well defined, extending approximately 500 km to the west of the western border of China. The borders of the Chinghai-Tibet subplate are coincident with zones of high seismic activity and fossil subduction (Molnar and Tapponier, 1975, 1977).

2) The North China subplate is bounded to the north by the Siberian platform (Hamilton, 1970), to the east by the Pacific Ocean, to the south by the Tsinling Shan, and to the west by the Ordos desert. The Tsinling Shan consists of a series of faults striking northwesterly into the Nanshan fold belt and is considered as both a distinct paleontogical and physical boundary between the two subplates. The Shansi graben consists of a series of northeast striking faults which extend north into the Ordos platform. These features are evident by LANDSAT-1 imagery as discussed by Cardwell and Isacks (1976). A major part of the North China subplate is the North China plain, a sediment-filled basin with an average

elevation of less than 100 meters, surrounded by uplifted areas of more than 1 km in elevation. Although the North China plain is considered an "intraplate" area, it has a long history of seismic activity as indicated by the Catalog of historical earthquakes in China (Lee, et al. 1976).

3) The South China subplate is south of the Tsinling Shan and east of the Tibetan and Tsaidam plateaus. It consists of the Yangtze fault block in the northwest and the South China fold block in the southeast (Sun and Teng, 1977). Its eastern boundary runs parallel to the shelf margin of the southeast coast of China, partially coincident with the subduction of the Pacific plate below the Eurasian plate. The presence of mélange in the east Coast Mountain Range of Taiwan, glaucophane in the Central Mountain Range of Taiwan (Sun and Teng, 1977), and considerable seismic activity in northeastern Taiwan (Katsumata and Sykes, 1969; Tsai, et al. 1978) have been used as evidence that this region is an active zone of subduction.

4) The Northwestern China subplate consists of the Tarim and Turfan basins, the Tien Shan fold belt, and the area north and west of the North China subplate. The regional tectonics of this area are not well known. A recent interpreation (Tapponier and Molnar, 1979) based on Landsat imagery and seismicity reveals the diversity of tectonics in the western portion of this subplate.

Date

The earthquakes used in the present study (Table 1) were chosen such that a major portion of their wave paths fall within the four major subplates of China (Fig. 2). A number of earthquakes are used for each path in order to obtain an estimate on the data repeatability and observational uncertainties. The path lengths range from approximately 1700 km to over 5000 km. For the path Tangshan to Taipei, the accuracy of surface wave data for periods greater

than 64 seconds was limited. All events in this study were recorded at two Seismological Research Observatory (SRO) stations located in Mashad, Iran (MAIO) and Taipei, Taiwan (TATO).

SRO data in digital form on tape is convenient for computer processing. The SRO stations operate at high sensitivity levels, thus expanding the detection threshold for seismic events and making small-magnitude events ($M \sim 5$) useful for long- and short- period surface wave dispersion analysis. Each seismic event must be decoded and plotted from the data tapes. Pure Love and Rayleigh waves are obtained by rotating the data coordinates. An example of a plotted seismic event, unrotated and rotated, is given in Figs. 3 and 4. A compllete discussion of handling SRO data can be found in Peterson, et al. (1976).

Method

A multiple filtering analysis (Dziewonski and Hales, 1970; Herrmann, 1973; Tung, 1974; Seekins and Teng, 1976) has been applied to the surface-wave train to obtain group velocity dispersion curves. A typical contoured result of the relative amplitude of wave energy arrivals over the path Tangshan to Taipei is shown for both the Rayleigh and the Love components in Figs. 5, 6 and 7. In these figures the dots represent the average group velocities obtained from the multiple filtering analysis. At the low-period end (below 20 seconds) ambiguity often arises in drawing contours due to interference by S waves. The contour lines will give several local maxima and will not allow a clearcut determination of group velocity values. The average dispersion curves for Rayleigh and Love components are plotted for all events of each path in Fig. 8-15. Higher-mode data are included when they are observable from the multifilter analysis. The observed data over each path are listed in Tables 2, 3, 4 and 5.

The inversion of the surface wave dispersion data for determining earth structure is based on the Backus-Gilbert inversion method (1967, 1968, 1970). Detailed descriptions of this method have been presented (Jackson, 1972; Wiggins, 1972; and Crosson, 1976). The basic logic of the inversion theory and some experience in its numerical applications will be briefly discussed as follows.

The observations, Y_i, are related to certain model paramters, X_j, in some known way, $Y_i = A(X_1, X_2, \ldots X_p)$. A quasi-linear relationship is established by taking a Taylor series expansiun about some initial value X'_0 .

$$Y_i = A_i\ (X'_0) + \frac{\partial A_i}{\partial X_j}\Big|_{X'_0} \Delta X_j \ + \text{higher order terms} \qquad (1)$$

where $Y_i = A_i\ (X'_0) + \Delta Y_i$

Ignoring the higher order terms, we obtain the function relationship in matrix form:

$$A\Delta X = \Delta Y$$

where ΔY_i = observed data minus calculated values, and A is a matrix whose elements are the partial derivatives in Equation 1. ΔX is a p x 1 vector whose elements are corrections to the initial model X'_0. ΔY is the difference between the observed and theoretical values.

In the present case the observations are group velocities of Love and Rayleigh waves, and the model parameters are shear velocities and densities for a horizontally layered earth. The partial derivatives in equation 1 are generated numerically by the method described by Rodi et al. (1975).

The classic least squares solution to equation 2 is by minimizing the Euclidean length of $A\Delta X-\Delta Y$, or

$$|| A\Delta X-\Delta Y || = (A\Delta X-\Delta Y)^T(A\Delta X-\Delta Y)= \epsilon$$

Given equation 2, the solution is (Hanson and Lawson, 1975):

$$A\Delta X = \Delta Y$$

$$A^TA\Delta X = A^T\Delta Y$$

$$\Delta\hat{X} = (A^TA)^{-1}A^T\Delta Y$$

where $\Delta\hat{X}$ is the estimated correction vector.

A suitable inverse to this problem can be obtained by using the singular value decomposition (SVD) of the matrix A.

$$A = U\Lambda V^T$$

where the columns of U are the eigenvectors associated with the columns of A, the rows of V are the eigenvectors associated with the rows of A, and Λ is a diagonal matrix of non-zero eigenvalues of the matrix A.

$$\Lambda = A^TA = \begin{vmatrix} \lambda_1 & \cdot & \cdot & \cdot & \cdot \\ 0 & \lambda_2 & \cdot & \cdot & \cdot \\ \cdot & \cdot & \cdot & \cdot & \cdot \\ 0 & \cdot & \cdot & \cdot & \lambda_n \end{vmatrix}$$

If we let

$$H = (A^T A)^{-1} A^T \tag{3a}$$

then

$$HA\Delta X = H\Delta Y \tag{3b}$$

and

$$\Delta\hat{X} = HA\ X \tag{3c}$$

and

$$\Delta\hat{X} = H\Delta Y$$

Using the SVD we obtain (Jackson, 1972):

$$\Delta\hat{X} = (\Lambda V^{-1} U^T)\Delta Y \tag{3d}$$
$$H = \Lambda V^{-1} U^T$$

Here, H is known as the pseudo-inverse of equation 2.

The matrix product HA=R is known as the resolution matrix, and is a measure of the uniqueness of the solution (Jackson, 1972). The rows of R are called the resolving kernels. From equation 3c it can be seen that an element of $\Delta\hat{X}$, $\Delta\hat{X}_i$, may be interpreted as convolving the i^{th} row of R with the vector ΔX. Therefore, ΔX_i can be considered the weighted sum of nearby values (Jackson, 1972).

Because $A^T A$ is nearly singular, a number of problems arise: (1) The solution vector becomes large, which can cause the problem to leave the region of linearity; (2) the solution oscillates with each iteration. By looking at the pseudo-inverse H we can see the cause of this instability.

$$H = \Lambda V^{-1} U^T$$

where the matrix Λ^{-1} equals

$$\Lambda^{-1} = \begin{vmatrix} \frac{1}{\lambda_1} & 0 & \cdots & & \\ 0 & \frac{1}{\lambda_2} & 0 & \cdots & \\ \cdots & \cdots & \cdots & \cdots & \\ \cdots & \cdots & \cdots & \cdots & \\ 0 & \cdots & \cdots & \cdots & \frac{1}{\lambda_n} \end{vmatrix}$$

and the λ_i's are the eigenvalues of the matrix A^TA. If A^TA is near singular, one or more of the eigenvalues will be approaching zero. From equation 3 it can be seen that a small eigenvalue will cause a large change in one or more values of the correction vector $\Delta\hat{X}$. Similarly, it has been shown that the variance of the model parameters are inversely proportional to λ (Jackson, 1972). Thus, small λ's produce large standard deviations.

There are two main approaches to stabilizing the inversion process. One method is to examine the eigenvalue spectrum of the matrix A. Small eigenvalues are removed when the variance becomes too large, but removing the eigenvalues degrades the resolution. This trade-off between resolution and variance has been discussed by a number of authors (Jackson, 1972; Wiggins, 1972; and Crosson, 1976). Braille and Keller (1975) used this method for the inversion of group velocity data.

Inversion stability can also be achieved by using Marquardt's method (Marquardt, 1963) or the stochastic inverse (Franklin, 1970). These procedures lead to the suppression of small eigenvalues. Franklin's stochastic inverse estimates the parameter in the presence of noise.

$$A\Delta X + n = \Delta Y \tag{4}$$

Where n is a vector of observational noise, Franklin (1970) shows that the solution to equation 4 is given by:

$$\Delta X = WA^T(AWA^T + ED)^{-1}\Delta Y \tag{5}$$

where W is the covariance matrix of the parameter and ED is the covariance matrix of the observations.

Marquardt's method considers a minimization of the functional

$$(A\Delta X - \Delta Y)^T(ED^TED)\ (A\Delta X - \Delta Y) - \Delta X^T IW^TW)\ \Delta X \tag{6}$$

with the solution given by:

$$\Delta X = (A^TED^{-1}\ A + W^{-1})^{-1}A^TED^{-1}\ Y \tag{7}$$

Letting $A^TED^{-1} = A^T$, equation 7 becomes:

$$\Delta X = (A^TA + \sigma^2 I)\ \ A^T\Delta Y \tag{8}$$

where σ^2 is the variance of the parameter.

By looking at the SVD of equation 8 we can see how Marquardt's method tapers the eigenvalue spectrum:

$$\Delta X = V|\ (\Lambda^2 + \sigma^2 I)^{-1}\Lambda|U^T\Delta Y \tag{9}$$

An element in brackets from equation 9 equals: (Crosson, 1976).

$$|(\Lambda^2 + \sigma^2 I)^{-1}\Lambda|_i = \lambda_i/(\lambda^2_i + \sigma^2)$$

So as λ_i approaches zero, the parameter ΔX_i also approaches zero. A similar analysis for the stochastic inverse shows that it too suppresses small eigenvalues.

The quantity σ^2 can also be thought of as a tradeoff parameter between resolution and variance (Der et al., 1970; Wiggins, 1972; Crosson, 1976). In Marquardt's method, the resolution equals (Crosson, 1976):

$$R = HA = (A^TA + \sigma^2 I)A^TA = V|(\Lambda + \chi^2 I)^{-1}\Lambda^2|V^T \quad (10)$$

For the stochastic inverse

$$R = |(\Lambda^2 + \sigma^2 I)^{-1}|\Lambda^2 VV^T \quad (11)$$

The quantity in brackets of equations 10 and 11 is a diagonal matrix whose elements have the form:

$$\lambda_i^2/(\lambda^2 + \sigma^2)$$

If $\sigma^2 = 0$, then $R = I$, but as σ^2 approaches zero, then the variance of the parameters becomes larger. We then adjust the size of σ^2 until there is an acceptable trade-off between standard deviation and resolution.

Two other elements that must be analyzed in the iversion process are the apriori (SDX_0) and a posteriori (SDX) standard deviations of the inversion parameters:

$$SDX_0 = \sqrt{D^T(\sigma W^{-1})D}$$

$$SDX = \sqrt{D^T(A^T E D^{-1} A + \sigma W^{-})D}$$

where D = a row vector of a delta matrix = (0,0,...,1,0,...,0). This analysis will give a measure of how much new information is coming from the data. SDX_0 is the standard deviation of the initial model paramters before inversion, whereas SDX is the standard deviation calculated from the data after inversion. If SDX_0 and SDX are approximately the same, we know that very little additional information is coming from the data.

The advantages of Marquardt's method and the stochastic inverse are that (1) the SVD of A is not explicitly determined, and (2) there is no decision to be made on the range of the matrix A^TA.

A combination of these two methods is used in our inversion process. When the number of parameters is greater than the number of data, the stochastic inverse is used. If the number of observations is greater than the number of parameters, Marquardt's method is used. This procedure leads to the minimum number of computations.

Results and Discussion

Initial models for the inversion were based on the results of a previous surface wave study done by Tung (1974). Starting models for all paths were initially inverted for both shear velocity and density. During the inversion, large instabilities of the density parameter were found in the crust. This was corrected by changing the starting model and inverting for the compressional wave velocity with the shear velocity and density. As discussed by Wiggens (1972), Der, et al. (1978), and Jackson (1976), the partial derivatives for shear velocity are larger than those for compressional velocity or density. Therefore the resolution for shear wave velocity is considerably better than the other two parameters. Only the resolution matrix for the partial derivatives with respect to shear velocity shall be presented.

1. Chinghai-Tibetan Plateau and Hindukush Region

Two separate paths across the Tibetan plateau were used (Fig. 2). Both paths originate from earthquakes located on the eastern boundary of the Tibetan plateau. Approximately 3/4 of the paths encompass the Chinghai-Tibetan subplate. The first group occurred in Szechwan province and the second group occurred to the south in Yunnan Province. A list of the surface waves is presented in Table 1. For each path across the Tibetan plateau inversions were performed using the fundamental and first higher mode Rayleigh waves. A fit of the theoretical model to the observed group velocity is presented in Figs. 16 and 17. A comparison between the average continental dispersion for Rayleigh waves (Ewing, et al. 1957) and Rayleigh waves for the four paths across China are presented in Fig. 18. The group velocities across the Tibetan plateau are substantially lower

than the group velocities for the average continental structure, with differences extending to periods of 120 seconds, indicating abnormal upper mantle structure.

Group velocities across the Tibetan plateau are the lowest of all the regions of China. Rayleigh wave group velocities ranged between 2.60 to 3.65 km/sec and steep slopes occurred in the dispersion curves between 40 to 60 seconds, where the change in group velocity was as high as 0.6 km/sec. Love waves were not used in the inversions due to the absence of amplitude maxima in the dispersion curves between 30 to 60 seconds. Earlier studies (Thatcher and Brune, 1969; James, 1971) have discussed the problem of interference of Love waves crossing inhomogeneous media. Tung (1974) attributed this problem on the Tibetan plateau to Love waves following a non-least time path. A possible structural implication is that there may be structures along the path corresponding to wave lengths of the Love waves, causing the wave energy to travel along a non-least time path with slower velocities.

Starting and final shear wave velocity models with standard deviation bars for the path Szechwan to Mashad are presented in Figure 19. Table 6 presents the initial and final model parameters and the resolution matrix for each model. The resolution matrix for the eight-layer model is presented in Table 7. From the width of the resolving kernels it is possible to resolve layers of 15 km in the upper crust, 15-20 km in the middle crust, and 25-30 km in the lower crust.

Starting and final shear wave velocity models with standard deviation bars for the path Yunnan to Mashad are presented in Figure 20. Tables 8-9 present the initial and final model parameters and the resolution matrix. From the width of the resolving kernels it is possible to resolve a 10-15 km layer at the top of the crust, 15-20 km layer in the middle of the crust, and a 20-25 km layer at the base of the crust.

Resolution in the mantle is poor for both paths. The standard deviations were found to be less than 0.15 km/sec for all the models presented. Increasing the resolution in the crust and mantle leads to both large standard deviations and instabilities in the shear wave velocity model (Rosenthal, 1977). A measure

of the amount of new information obtained from the data is given by comparing the magnitudes of the apriori standard deviation (SDX_0) to the a posteriori standard deviations (SDX) given in Tables 7 and 9. In the upper mantle there is only a small amount of new information being obtained from the data, and the final model, including the location of the Moho, is most affected by the starting model. As a result, a low velocity layer in the upper mantle can only be inferred from the small amount of new information being obtained. Additional data for periods longer than 120 seconds and good Love wave data would significantly increase the amount of new information.

The shear wave velocity structure for both paths crossing the Tibetan plateau is similar. The crust is approximately 70 km thick and may be broken into four layers. The first layer has shear velocities that range between 2.87-3.06 km/sec, suggesting a layer approximately 15 km thick of partly sedimentary origin. Tung (1974) and Mu, et al. (1974) discussed the existence of thick sedimentary layers in the Mount Jolmo Lungma (Mount Everest) region of the Himalayas. Both Birch (1963) and Simmons (1964) reported shear velocities for sedimentary rocks at 10 to 15 km depth of approximately 3.00 to 3.08 km/sec. A second layer has shear wave velocities ranging from 3.20 to 3.40 km/sec and is approximately 15 km thick, suggesting a layer of granitic or equivalent composition. A third layer has shear velocities between 3.40 to 3.70 km/sec, is approximately 15 to 20 km thick, and also seems to consist of granite. For comparison, Birch and Bancroft (1958), Birch (1963) and Simmons (1964) reported shear velocities for granite under 3 to 5 kilobars of pressure of 3.45-3.70 km/sec. Simmons (1964) reported that granite with a shear wave velocity of 3.56 km/sec at 4 kilobars pressure has a shear wave velocity of 3.79 km/sec at pressures of 10 kilobars. The fourth layer with shear wave velocities between 3.85 to 3.95 km/sec corresponds to granite at pressures of approximately 20 kilobars, which would correspond to depths of 60 to 70 km.

The dispersion curves and shear wave velocity profile for the Tibetan plateau is in agreement with those values presented by Tung (1974) and Bird

of the amount of new information obtained from the data is given by comparing the magnitudes of the apriori standard deviation (SDX_0) to the a posteriori standard deviations (SDX) given in Tables 7 and 9. In the upper mantle there is only a small amount of new information being obtained from the data, and the final model, including the location of the Moho, is most affected by the starting model. As a result, a low velocity layer in the upper mantle can only be inferred from the small amount of new information being obtained. Additional data for periods longer than 120 seconds and good Love wave data would significantly increase the amount of new information.

The shear wave velocity structure for both paths crossing the Tibetan plateau is similar. The crust is approximately 70 km thick and may be broken into four layers. The first layer has shear velocities that range between 2.87-3.06 km/sec, suggesting a layer approximately 15 km thick of partly sedimentary origin. Tung (1974) and Mu, et al. (1974) discussed the existence of thick sedimentary layers in the Mount Jolmo Lungma (Mount Everest) region of the Himalayas. Both Birch (1963) and Simmons (1964) reported shear velocities for sedimentary rocks at 10 to 15 km depth of approximately 3.00 to 3.08 km/sec. A second layer has shear wave velocities ranging from 3.20 to 3.40 km/sec and is approximately 15 km thick, suggesting a layer of granitic or equivalent composition. A third layer has shear velocities between 3.40 to 3.70 km/sec, is approximately 15 to 20 km thick, and also seems to consist of granite. For comparison, Birch and Bancroft (1958), Birch (1963) and Simmons (1964) reported shear velocities for granite under 3 to 5 kilobars of pressure of 3.45-3.70 km/sec. Simmons (1964) reported that granite with a shear wave velocity of 3.56 km/sec at 4 kilobars pressure has a shear wave velocity of 3.79 km/sec at pressures of 10 kilobars. The fourth layer with shear wave velocities between 3.85 to 3.95 km/sec corresponds to granite at pressures of approximately 20 kilobars, which would correspond to depths of 60 to 70 km.

The dispersion curves and shear wave velocity profile for the Tibetan plateau is in agreement with those values presented by Tung (1974) and Bird

and Töksoz (1977). Chun and Yoshi (1977), using Rayleigh and Love waves for many different paths across the Tibetan plateau, reported a crustal thickness of approximately 70 km and observed a velocity reversal in the middle crust. Due to a 15 to 20 km resolution in the middle crust, it is doubtful a velocity reversal could be observed for data over the two paths presented.

Due to the small amount of information (apriori vs. a posteriori standard deviations) derived from inverting Rayleigh waves in the upper mantle, the above structural conclusions are only tentative. The upper mantle shear velocities are lower than either the Gutenburg earth model (Tacheuchi, et al. 1964) or the Brune and Dorman (1963) model for the Canadian Shield (Fig. 21). The velocity at the top of the mantle is approximately 4.4 km/sec, with indications of a low velocity layer at about 90 km depth. Since the low velocity layer can only be inferred, the existence of extremely low velocities of 4.1 km/sec is tenative. Low shear velocities in the upper mantle of Tibet have been reported by Tung (1974), which suggests a high degree of partial melting and a low resistance to deformation (Anderson, et al. 1972).

2. North and Northwestern China

The path between Tangshan and Mashad, Iran (Fig. 2) crosses the North China subplate and the Northwestern China subplate including the Tien Shan fold belt. Tung (1974) found crustal thicknesses of 30, 40 and 45 km for Northeast, Central and Northwest China respectively. Crustal thicknesses in the Tien Shan and Pamir Mountains have been reported as high as 65 km (Arkhangel'skaya, 1964).

A list of the earthquakes and surface wave trains used over the path Tangshan to Mashad, Iran are listed in Table 1. The fit of the theoretical to observed group velocities for the Rayleigh and Love waves is given in Fig. 22. The theoretical Rayleigh wave group velocity is lower than the average continental Rayleigh wave dispersion (Ewing, et al. 1957). Starting and final shear wave velocity models with standard deviation bars are presented in Fig. 23. Tables 10 and 11 present the starting and final model parameters and the resolution

matrix. From the width of the resolving kernels presented in Table 11, it is possible to resolve a 10 km layer at the top of the crust, 10 to 15 km layer in the middle of the crust, and a 20 km layer at the base of the crust.

When Rayleigh and Love waves are inverted simultaneously, a considerable amount of new information may be derived from the data. Observing the magnitude of the apriori (SDX_0) vs. the a posteriori (SDX) standard deviations, a considerable amount of new information is obtained at depths of 100 km (seventh layer). Below this depth, less new information is obtained from the data, and the final model is most affected by the starting model.

The average crustal thickness over the path from Tangshan to Mashad is approximately 45 km. Since this path is not considered a pure path, only average shear velocities are presented (Fig. 2). A three-layer crust seems to be an adequate model for this path. The first layer is approximately 10 km thick and has an average shear velocity of approximately 3.0 km/sec, suggesting a layer at least partly sedimentary (Birch, 1963; and Simmons, 1964). The second layer is 15 to 20 km thick and has an average shear wave velocity of 3.55 km/sec. The layer at the base of the crust, 20 to 25 km thick, has an average shear velocity of approximately 3.80 km/sec, suggesting a layer of granitic origin (Birch, 1963; Simmons, 1964). The average shear wave velocity at the top of the mantle is 4.40 to 4.45 km/sec and the low velocity layer begins at approximately 90 km. Using a three-layer earth model proposed by Dorman (1959), Schechkov (1961) was able to fit mixed path dispersion data for Northwest China to a theoretical three-layer model of average crustal thickness of 50 km: the first layer has a shear velocity of 3.40 km/sec and is 20 km thick, the second layer has a 3.53 km/sec shear velocity and is 30 km thick, and a semi-infinite third layer has a 4.50 km/sec shear velocity for the mantle. Applying the concept of regionalization to paths crossing Northwest China, Tung (1974), presented a three-layer crust of 45 km thickness. Shear velocities calculated by Tung (1974) for the crust and upper mantle are lower than the mixed path average shear velocities presented. The low velocity zone presented is not as prominent as Tung (1974) reported, and can only be inferred from the

information obtained from the data.

A comparison of the Canadian Shield model (Brune and Dorman, 1963) with the average shear velocity model for Tangshan to Mashad is presented in Fig. 24. Both models have higher shear velocities in the crust and at the top of the mantle than the theoretical model presented for the path Tangshan-Mashad. The tectonics over the path between Tangshan-Mashad may account for the lower velocity at the top of the mantle. The catalog of historical earthquakes presented by the Chinese Institute of Geophysics Academia Sinica (Lee, et al. 1976) shows considerable seismic activity throughout the regions traversed by the surface waves. Successive stages of subduction of the Indian plate below the Eurasian plate are believed to have taken place in areas as far north as the Tarim basin and Mongolia (Chang and Zeng, 1973; Zonenshain, 1973). These are consistent with a thicker crust, lower group velocities and lower shear velocities in the upper mantle. These results suggest that the origin of the Tien Shan fold belt may also be a result of the collision of the Eurasion and Indian plates.

3. Coastal China

For most of the path between Tangshan to Taipei the surface waves are parallel to the east coast of China. According to the tectonic map of the Institute of Geology of The Chinese Academy of Sciences from which Fig. 1 is derived, the crustal thickness along most of the path is about 30 km. A starting model for inversion was chosen to reflect the 30 km crustal thickness. A list of the earthquakes and surface wave trains used in the analysis is given in Table 1. The fit of the theoretical to the observed Rayleigh and Love wave group velocities is presented in Fig. 25. A comparison between the theoretical Rayleigh and the average continental Rayleigh wave group velocities (Ewing, et al. 1957) shows lower group velocities of both short and intermediate periods.

The starting and final shear wave velocity models with standard deviation bars are presented in Fig.26. The shear velocity parameters and resolution matrix

are presented in Tables 12 and 13. From the width of the kernels of the resolution matrix (Table 13), it is possible to resolve a 5 to 7 km layer at the top of the crust, a 10 km layer in the middle of the crust, and a 15 to 20 km layer at the base of the crust. An examination of the apriori (SDX_0) and a posteriori (SDX) standard deviations indicates that a small amount of information exists in the data below the fifth layer. Thus longer period data is needed for increased information in the mantle. Since the path length from Tangshan to Taipei is approximately 1700 km, with the present analysis periods greater than 64 seconds will not have proper mode separation. Consequently, it is unlikely that for this path new information below the top of the mantle can be obtained and shear velocity in the mantle is most affected by the starting model.

A crust with a thickness of 30 km and composed of three layers ia an adequate model for the structure over the path. The first layer, approximately 5 to 7 km thick, seems to be a sedimentary layer with shear velocity of approximately 2.95 km/sec. The second layer is $\sim$10 km thick. The third layer, approximately 15 to 20 km thick, corresponds to s shear velocity of approximately 3.85 km/sec. in the mantle, a low velocity layer can only be inferred due to the lack of sufficient information from the data. A comparison of the Canadian Shield model (Brune and Dorman, 1963) and the Gutenberg earth-model (Tacheuchi, et al. 1964) with the shear velocity profile shows higher velocities in the mantle and the base of the crust (Fig. 27).

The shear velocity of 4.46 km/sec. at the top of the mantle is lower than the shear velocity of the Canadian Shield (4.65 km/sec.). Tung (1974) also calculated a mantle shear velocity of 4.42 km/sec. at the top of the mantle for a path crossing Northeast China recorded in Hong Kong. The tectonics over the path from Tangshan to Taipei explains the lower velocities in the mantle.

The region traversed is considered an "intraplate" region, although a considerable amount of seismic history is evident from the catalog of historical earthquakes compiled by the Chinese Institute of Geology Academia Sinica (Lee, et al. 197

For example, in the northeastern portion of the South China subplate is the Tanlu fault, which may be traced from Landsat photographs (Lee, et al. 1976) northward across the border with the North China subplate, through Shantung Province, the Pohai Gulf and into Liaoning Province (north of Tangshan). The Tangshan earthquake (July 1976) and the Haichang earthquake (February 1975) indicate that the northern portion of the path from Tangshan to Taipei passes through a tectonically active region.

The southern portion of the path traverses a region affected by the Philippine Sea plate that is subducted beneath the Eurasion plate. The tectonics of this region have been discussed by Sun and Teng (1977). Considerable seismic activity is found throughout northern and eastern Taiwan, particularly along a major north-south trending fault paralleling the east coast of Taiwan. Sun and Teng (1977) discussed the importance of this fault to a subduction zone of Mesozoic or Cenozoic age. The eastern provinces of Fuchien, Kiangsu, Chiekiang, Kwantung, Anhwai and Kiangsi are covered by large-scale volcanic intrusions which are of Mesozoic age. These volcanic intrusions are attributed to a magma source as a consequence of the melting from the subduction of the Pacific Sea plate. Finally, higher than normal heat flow (3 to 4 heat flow units) has been observed north of Taiwan which is associated with areas of plate subduction (Yansuii, et al. 1970). All these factors would contribute to a shear wave velocity profile lower than normal in the upper mantle.

Conclusions

By using a multiple-filter technique, group velocities for various regions of China were obtained from earthquakes recorded at SRO stations in Mashad, Iran and Taipei, Taiwan. For each sampling path, a number of events were used with practically the same source-station geometry to derive the dispersion data. An estimate of uncertainty of the data was thus obtained. A nonlinear least square technique was

used to invert the surface wave group velocity for shear wave velocity structures. The findings concerning the nature of the crust and mantle are:

1. Group velocities obtained for the pure path across the Tibetan plateau are unusually low when compared with the average continental dispersion. Results of the inversion indicate that a 4-layer 70-km thick crust is an adequate model for the Tibetan plateau.

2. Group velocities for the mixed path between Tangshan and Mashad, Iran are lower than the average continental dispersion. Results of the inversion indicate that a 3-layer, 45 km thick crust is an adequate model.

3. Group velocities for the path between Tangshan and Taipei, Taiwan are closest of the three regions to average continental dispersion. Results of the inversion indicate that a 3-layer 30-km crust is an adequate model.

For all three models, the structure of the upper mantle from information provided by the data is tentative. In comparing the apriori (SDX_0) to the a posteriori (SDX) standard deviations in the mantle, it was observed that the final model was influenced by the starting model more than by the data. Attempts to increase the information from the data and the resolution result in either unacceptably large standard deviations or unstable shear velocity models. Only in the case of data for the path from Tangshan to Mashad, for which inversions were performed simultaneously for long period Rayleigh and Love waves, was adequate information obtained about the upper mantle.

Previous surface wave studies of China have applied a trial-and-error inversion approach to obtain a snear velocity model from Rayleigh wave group velocity data. Proper consideration has not been given to either the information obtained from the data, or the resolution. In all these studies the influence of the starting model upon the final model was not discussed, thus the validity of the estimated upper mantle shear velocities presented is rather questionable.

Both Rayleigh and Love waves should be inverted simultaneously to obtain more information from the data. This may not always be possible due to crustal

anisotrophy. Higher mode data are very important, but generally the excitation of higher modes is not strong for the shallow earthquakes used in this study. In this regard, future large earthquakes, in Tibet for instance, of intermediate focal depths would be important sources for higher mode data and they warrant special attention. Further, the dispersion curves must not be contaminated by surface waves traveling non-least time paths or by complex structure along the path. This often presents a problem in tectonically active regions, resulting in the inability to obtain a good Love wave dispersion curve from the data. Finally, the problems due to epicentral distance must be considered. If the epicentral distance is too short, proper surface wave mode separation will not be achieved. Only after those factors are considered can one arrive at a better shear wave velocity structure by means of surface wave inversion for a specific geological province.

ACKNOWLEDGEMENT

This research was supported by the Advanced Research Project Agency of the Department of Defense and was monitored by the Air Force Office of Scientific Research under Contract No. F49620-76-C-0010. Helpful discussions with Drs. David Jackson and William Rodi are gratefully acknowledged.

REFERENCES

Anderson, D.L., Sammis, C. and Jordan, T. (1972). Composition of the Mantle and Core, The Nature of the Solid Earth: Edited by E.L. Robertson, McGraw Hill, 1972, p. 677.

Arkhangel'skaya, V.M. 1964). A Study of Short Period Surface Seismic Rayleigh Waves II: Izvestiya Acad. Sci. USSR Geophys. Ser., p. 807-821, English Translation.

Backus, G. and Gilbert, F. (1967). Numerical Application of a Formalism for Geophysical Inverse Problems: Geophys. J. 13, p. 247-276.

Backus, G. and Gilbert, F. (1968). The resolving Power of Gross Earth Data: Geophys. J. 16, p. 169-205.

Backus, G. and Gilbert, F. (1970). Uniqueness in the Inversion of Inaccurate Gross Earth Date: Phil. Trans. Roy. Soc. (London), Ser. A266, p. 123-192.

Birch, F. (1963). Some Geophysical Applications of High Pressure Research in Solids Under Pressure: edited by W. Paul and D.M. Warschauer; McGraw-Hill Book Company, New York, 1963.

Birch, F. and Bancroft, D. (1938). The Effect of Pressure on the Regidity of Rocks: J. Geol., 46, p. 59-83, 113-141.

Bird, P. and Toksöz, M.N. (1977). Strong Attenuation of Rayleigh Waves in Tibet: Nature, V266, p. 163-165.

Brune, J.N. and Dorman, J. (1963). Seismic Waves and Earth Structure in the Canadian Shield: Bull, Seism. Soc. Am. v. 53, p. 167-210.

Burrett, C. (1974). Plate Tectonics and Fusion of Asia: Earth and Planet. Sci. Letters; v. 21, p. 181-189.

Cardwell, R.K. and Isacks, B.L. (1976). Investigation of the 1966 Earthquake Series in Northern China Using the Method of Joint Epicenter Determination: Bull. Seism. Soc. Am. v. 66, p. 1965-1982.

Chang, C.F. and Zeng, S.L. (1973). Tectonic Features of the Mount Jolmo Lungma Region in Southern Tibet, China: Scientia Geologica Sinicia; no. 1, p. 1-12.

Chinese Academy of Sciences (1974), A Preliminary Note on the Basic Tectonic Features and Their Developments in China: Scientia Geologica Sinica; no. 1, p. 1-17.

Chun, K.Y. and Yoshii (1977). Crustal Structure of the Tibetan Pleateau, the Himalayas, and the Gangetic Basin: Trans. Am. Geophys. Un., v. 48, no. 6, p. 447.

Crossen, R.S. (1976). Curstal Structure Modeling of Earthquake Data 1, Simultaneous Least Squares Estimation of Hypocenter: J. Geophys. Res., 81, p. 3030-3046.

Der, Z., Masse, R. and Landisman, M. (1970). Effects of Observationsl Errors on the Resolution of Surface Waves at Intermediate Distances: J. Geophys. Res. 75, p. 3399-3409.

Dewey, J.F. and Bird, J.M. (1970a), Mountain Belts and the New Global Geotectonics: J. Geophys. Res. 73 p. 2625.

Dewey, J.F. and Bird, J.M. (1970b), Plate Tectonics and Geosynclines: Tectonophysics, 10 p. 265.

Dorman, J. (1959). Numerical Solution for Love Wave Dispersion on a Half Space with a Double Surface Layer: Geophysics, 24, p. 12-19.

Ewing, W.M., Jardetzky, W.S. and Press, F. (1957). Elastic Waves in Layered Media: McGraw-Hill Book Co., p. 380.

Hamilton, W. (1970). The uralides and Motion of the Russion and Siberian Platforms: Geol. Soc. Am. Bull., 81, p. 2553.

Hermann, R.B. (1973), Some Aspects of Band-pass Filterting of Surface Waves: Bull. Seism. Soc. Am., V. 63, p. 663-671.

Jackson, D.D. (1972). Interpretation of Inaccurate, Insufficient, and Inconsistent Data: Geophys. J. Roy. Astron. Soc., 28, p. 97-109.

Jackson, D.D. and Burkhard, N.R. (1976), Density and Surface Wave Inversions: Geophys. Res. Let. V. 3, No. 11, p. 637-638.

James, D.E. (1971). Anomalous Love Wave Phase Velocities: J. Geophys. Res. 76, p. 2077-2083.

Jell, P.A. (1973), Middle Cambrian Geography Deduced from an Analysis of Trilobite Distributions: Nature, 240, p. 288.

Katsumata, Mand Sykes, L.R. (1969). Seismicity and Tectonics of the Western Pacific: Izu-Mariana-Cardine and Ryukyu-Taiwan Regions: J. Geophys. Res., 74, p. 5923-5948.

Lee, W.H.K., Wu, F.T. and Jacobsen, C. (1976). A Catalog of Historical Earthquakes in China Compiled from Recent Chinese Publications: Bull, Seism. Soc. Am., V. 66, p. 2003-2016.

McElhinny, M.W. (1973), Paleomagnetism and Plate Tectonics of Eastern Asia, in The Western Pacific, ed. by P.J. Coleman, Univ. West. Austr. Press, p. 407.

Molnar, P.T. and Tapponier, P. (1975). Cenozoic Tectonics of Asia: Effects of a Continental Collision: Science, 189, p. 419-426.

Molnar, P.T. and Tapponier, P. (1977), The Collision Between Indian and Eurasia: Sci. Am., V. 236, No. 4, p. 30-41.

Mu, E.Z., Vin, J.X., Wen, S.X., Wang, Y.G. and Zhang, G.G. (1973), Stratigraphy of the Mount Jolmo Lunga Region in Southern Tibet: Chinese Scientia Geologica Sinica, no. 1, p. 13-25.

Peterson, J. Butler, H.M., Holcomb, L.G., and Hutt, C.R. (1976), The Seismic Research Observatory: Bull. Seism. Soc. Ams., 66, p. 2049-2074.

Rodi, W. L., Glover, P., Li, T. M. C., and Alexander, S. S., (1975), A Fast Accurate Method for computing Group-Velocity Partial Derivatives for Rayleigh and Love Modes: Bull. Seismol. Soc. Am. 65, p. 1105-1114.

Rosenthal, R. and Teng, T. (1977), Crustal and Upper Mantle Velocity and Q Structure of Mainland China: University of Southern California Geophysical Laboratory, Tech. Report, 77-5.

Savarensky, E. F. and Shechkov, B. N. (1961). The Structure of the Earth's Crust in Siberia in the Far East from Love Wave and Rayleigh Wave Dispersion: Izvestiya Acad. Sci. USSR Geophys. Ser., p. 454-456, English Translation.

Shechkov, B. N. (1964). Seismic surface Dispersion and Eurasian Crustal Structure: Izvestiya Acad. Sci. USSR Geophys. Ser., p. 183-187, English Translation.

Shechkov, B. N. (1961), Structure of the Earth's Crust in Eurasia from Dispersion of the Surface Waves: Izvestiya Acad. Sci. USSR Geophys. Ser., p. 450-453, English translation.

Simmons, G. (1964), Velocity of Shear Waves in Rocks to 10 kilobars: J. Geophys. Res. 69, no. 6, p. 1123.

Sun, N. C. and Teng, T. (1977), Tectonic Plates of China: University of Southern California, Geophysical Laboratory, Tech. Report, 77-4.

Tacheuchi H., Dorman, J. and Saito, M. (1964). Partial Derivatives of Surface Wave Phase Velocity with Respect to Physical Parameter Changes within the Earth: Geophys. Res., 69, p. 3429.

Tapponier, P. and Molnar, P. T. (1979), Active Faulting and Cenozoic Tectonics of the Tien Shan, Mongolia, and Baykal Regions, J. Geophys. Res., 84, B7, p. 3425-3459.

Thatcher, W. and Brune, J. N. 91969), Higher Mode Interference and Observed Anomalous Apparent Love Wave Velocities, J. Geophys. Res. 74, p. 6603-6611.

Töksoz, M. N. and Anderson, D. L. (1966), Phase Velocities of Long Period Surface Waves and Structure of the Upper Mantle: J. Geophys. REx., 71, p. 1649.

Tsai, Y. B., Teng, T. L., Chin, J. M., and Lin, H. L., (1978), Tectonic Implications of the Seismicity in the Taiwan Region Memoir of the Geological Society of China, No. 2, p. 13 - 41.

Tung, J. P. (1974), The Surface Wave Study of Crustal and Upper Mantle Structure of Mainland China: Ph.D. dissertation, University of Southern California, 248 p.

Whittington, H. B. and Hughes, C. P. (1972), Ordivician Geography and Faunal Provinces: Phil. Trans. Roy. Soc. London, 263, p. 235.

Wiggins, R. A., (1972). The General Linear Inverse Problems: Implications of Surface Waves and Free Oscillations for Earth Structure: Rev. Geophys. Space Phys., 10, p. 251-285.

Yasuii, M. Epp, D., Nagasaka, and K., Kishii, T., (1970). Terrestrial Heat Flow in the Seas Around Nansei Shoto (Ryukyu Islands): Tectonophysics, 10, p. 225-235.

Zonenshain, L. P. (1973), The Evolution of Central Asiatic Geosynclines through Sea-floor spreading: Tectonophysics, 19, p. 213-232.

TABLE 1 - Pertinent Earthquakes Information Used in this Study

Location	Origin Time	Station	M	Wave Type	Component	Path	Distance
39.9° N 118.0° E N.E. China	July 29, 1976 01:01:04.1	MAIO	5.1	Rayleigh Love	Vertical Transverse	Tangshan-Mashad	5119
39.8° N 117.8° E N.E. China	July 30, 1976 21:23:13.8	MAIO	5.4	Love	Transverse	Tangshan-Mashad	5072
39.6° N 117.9° E N.E. China	Aug. 2, 1976 09:16:00.5	MAIO	4.4	Rayleigh	Vertical	Tangshan-Mashad	5053
39.7° N 118.5° E N.E. China	Aug. 8, 1976 01:09:12.4	MAIO	4.9	Rayleigh Love	Vertical Transverse	Tangshan-Mashad	5100
40.2° N 118.9° E N.E. China	Aug. 8, 1976 22:41:34.3	MAIO	5.1	Rayleigh	Vertical	Tangshan-Mashad	5118
39.6° N 118.5° E N.E. China	Aug. 14, 1976 16:02:44.5	MAIO	4.7	Rayleigh Love	Vertical Transverse	Tangshan-Mashad	5103
32.753° N 104.157° E Szechwan	Aug. 16, 1976 14:06:45.9	MAIO	6.1	Rayleigh	Vertical Radial	Szechwan-Mashad	4080
32.893° N 104.189° E Szechwan	Aug. 19, 1976 12:49:47.7	MAIO	5.4	Rayleigh	Vertical Radial	Szechwan-Mashad	4078
32.571° N 104.152° E Szechwan	Aug. 21, 1976 21:49:54.2	MAIO	6.1	Rayleigh	Vertical Radial	Szechwan-Mashad	4095

TABLE 1 - (Continued)

Location	Origin Time	Station	M	Wave Type	Component	Path	Distance
32.492° N 104.181° E Szechwan	Aug. 23, 1976 03:30:7.6	MAIO	6.2	Rayleigh	Vertical Radial	Szechwan-Mashad	4088
32.460° N 104.152° E Szechwan	Sept. 1, 1976 01:06:51.8	MAIO	5.1	Rayleigh	Vertical Radial	Szechwan-Mashad	4090
24.343° N 98.642° E Yunnan	May 31, 1976 5:08:28.5	MAIO	5.5	Rayleigh	Vertical Radial	Yunnan-Mashad	3956
24.191° N 98.676° E Yunnan	July 3, 1976 16:33:23.1	MAIO	5.3	Rayleigh	Vertical Radial	Yunnan-Mashad	3967
39.8° E 118.6° E N.E. China	July 28, 1976 15:35:55.3	TATO	5.4	Rayleigh Love	Vertical Radial Transverse	Tangshan-Taipei	1661
39.8° N 118.9° E N.E. China	July 30, 1976 21:23:13.8	TATO	5.4	Rayleigh Love	Vertical Radial Transverse	Tangshan-Taipei	1670
39.6° N 117.8° E N.E. China	Aug. 1, 1976 20:53:53.6	TATO	4.6	Rayleigh Love	Vertical Radial Transverse	Tangshan-Taipei	1656
39.9° N 118.8° E N.E. China	Sept. 6, 1976 17:02:01.5	TATO	4.8	Rayleigh	Vertical	Tangshan-Taipei	1672

MAIO: Mashad, Iran 36.30° N 59.49° E

TATO: Tapei, Taiwan 24.976° N 121.489° E

TABLE 2

Tangshan-Taipei Observed Dispersion Data

Period (sec)	Rayleigh Wave (km/sec)	Love Wave (km/sec)
64.0	3.49 ± .06	3.85 ± .15
51.2	3.48 ± .09	3.71 ± .10
42.7	3.46 ± .11	3.69 ± .06
36.6	3.48 ± .11	3.59 ± .05
32.0	3.30 ± .09	3.52 ± .08
28.4	3.29 ± .05	3.37 ± .05
25.6	3.15 ± .08	3.31 ± .05
23.3	3.04 ± .05	3.19 ± .05
21.3	3.00 ± .06	3.19 ± .05
19.7	2.84 ± .06	3.12 ± .09
18.3	2.76 ± .09	3.12 ± .07
17.1	2.72 ± .06	3.04 ± .09
16.0	2.67 ± .05	3.02 ± .04
15.1	2.63 ± .10	2.93 ± .05
13.5	2.58 ± .13	2.89 ± .10
12.2	2.52 ± .10	2.85 ± .15
11.1	2.59 ± .18	2.90 ± .07
10.2	2.64 ± .17	2.91 ± .15

TABLE 3

Tangshan-Mashad Observed Dispersion Data

Period (sec)	Rayleigh Wave (km/sec)	Love Wave (km/sec)
102.4	3.73 ± .20	4.00 ± .20
85.3	3.65 ± .18	3.91 ± .13
73.1	3.69 ± .10	3.91 ± .10
64.0	3.57 ± .10	3.85 ± .05
56.9	3.65 ± .18	3.74 ± .06
51.2	3.54 ± .05	3.70 ± .11
46.5	3.47 ± .05	3.66 ± .10
42.6	3.43 ± .05	3.56 ± .06
39.4	3.35 ± .05	3.46 ± .05
36.6	3.22 ± .05	3.38 ± .05
34.1	3.14 ± .04	3.36 ± .05
32.0	3.10 ± .05	3.31 ± .05
30.1	3.01 ± .06	3.29 ± .06
26.9	2.93 ± .06	3.21 ± .05
24.4	2.91 ± .08	3.18 ± .05
22.3	2.85 ± .10	3.16 ± .07
20.5	2.74 ± .06	3.17 ± .05
18.9	2.78 ± .10	3.14 ± .05
16.0	2.82 ± .18	3.06 ± .06
13.8	2.75 ± .07	3.01 ± .06
12.2	2.79 ± .08	2.95 ± .10
10.9	2.69 ± .08	2.89 ± .15

TABLE 4

Yunnan-Mashad Observed Dispersion Data

Period(sec)	Rayleigh Wave(km/sec) Fundamental	First Higher Mode
102.4	3.52 ± .15	
85.3	3.49 ± .15	
73.1	3.41 ± .10	
64.0	3.25 ± .15	
56.9	3.12 ± .10	
51.2	3.05 ± .10	
46.5	3.00 ± .10	
42.7	2.95 ± .10	
39.4	2.87 ± .07	
36.6	2.79 ± .07	
34.1	2.73 ± .07	
32.0	2.71 ± .07	
30.1	2.73 ± .15	
27.0	2.67 ± .15	
24.4	2.85 ± .15	
22.3	2.79 ± .05	
20.5	2.79 ± .05	4.09 ± .15
18.9	2.77 ± .05	3.80 ± .17
16.0	2.77 ± .06	3.48 ± .10
13.8	2.77 ± .06	
12.2	2.64 ± .15	3.17 ± .08
10.9	2.71 ± .10	3.15 ± .07

TABLE 5

Szechwan-Mashad Observed Dispersion Data

Period(sec)	Rayleigh Wave(km/sec) Fundamental	First Higher Mode
102.4	3.54 ± .17	
85.3	3.56 ± .09	
73.1	3.49 ± .06	
64.0	3.41 ± .07	
56.9	3.28 ± .06	
51.2	2.96 ± .15	
46.5	2.96 ± .15	
42.7	2.95 ± .07	
39.4	2.87 ± .06	
36.7	2.87 ± .08	
34.1	2.87 ± .09	
32.0	2.79 ± .10	
30.1	2.76 ± .09	
26.9	2.75 ± .06	
24.4	2.74 ± .07	
22.3	2.76 ± .04	
20.5	2.69 ± .05	
18.9	2.71 ± .04	
16.0	2.73 ± .04	3.72 ± .20
13.8	2.70 ± .07	3.45 ± .15
12.2	2.73 ± .13	3.35 ± .15
10.8		3.16 ± .10

TABLE 6 : Model Fit for Path Szechwan-Mashad (8 Layers)

		Initial Model			Final Model		
Layer	H(km)	α(km/sec)	β(km/sec)	ρ(gr/cm)	β(km/sec)	SDX_o	SDX
1	15	5.55	2.80	2.70	3.06	0.189	0.046
2	15	5.60	3.20	2.90	3.28	0.189	0.070
3	25	6.40	3.30	3.00	3.67	0.147	0.063
4	20	6.60	3.80	3.10	3.98	0.164	0.114
5	25	7.50	4.45	3.30	4.39	0.164	0.140
6	25	7.20	4.20	3.35	4.31	0.147	0.128
7	25	7.20	4.10	3.36	4.18	0.147	0.137
8	25	7.20	4.20	3.37	4.21	0.147	0.143

TABLE 7 : Resolution Matrix for Path Szechwan-Mashad (8 Layers)

Layer	1	2	3	4	5	6	7	8
1	0.989	0.0007	0.007	0.001	0	0	0	0
2	0.007	0.951	0.029	-0.042	0.004	0.005	-0.001	0
3	-0.013	0.049	0.918	0.054	-0.084	-0.018	0.003	-0.004
4	0.001	-0.056	0.043	0.769	0.158	-0.055	-0.054	0.035
5	-0.008	0.006	0.067	0.158	0.456	0.250	0.021	-0.071
6	-0.004	0.008	-0.018	-0.069	0.313	0.435	0.255	0.063
7	-0.004	-0.002	0.004	-0.068	0.026	0.255	0.310	0.206

TABLE 8 : Model Fit for Path Yunnan-Mashad

		Initial Model			Final Model		
Layer	H(km)	α(km/sec)	β(km/sec)	ρ(gr/cm)	β(km/sec)	SDX_o	SDX
1	10	5.50	2.80	2.70	2.91	0.347	0.144
2	10	5.60	3.10	2.90	3.29	0.347	0.157
3	10	5.65	3.20	2.92	3.40	0.347	0.208
4	10	6.25	3.30	3.00	3.56	0.347	0.242
5	15	6.45	3.40	3.05	3.54	0.283	0.180
6	15	6.60	3.80	3.10	3.90	0.283	0.201
7	20	7.45	4.45	3.30	4.44	0.245	0.200
8	20	7.20	4.20	3.34	4.19	0.245	0.208
9	25	7.20	4.15	3.35	4.10	0,219	0.190
10	25	7.20	4.15	3.36	4.10	0.219	0.205
11	25	7.20	4.20	3.37	4.15	0.219	0.213

TABLE 9: Resolution Matrix for Path Yunnan-Mashad

Layer	1	2	3	4	5	6	7	8	9	10	11
1	0.926	0.163	-0.132	0.028	0.028	-0.001	0.002	0.003	0	0	0
2	0.163	0.839	0.194	-0.076	-0.021	-0.010	-0.008	-0.005	0.005	-0.004	-0.002
3	0.132	0.192	0.640	0.238	-0.011	0.020	0.001	-0.024	-0.016	-0.007	-0.003
4	0.028	-0.076	0.238	0.471	0,235	-0.072	-0.029	-0.001	-0.007	-0.010	-0.007
5	0.039	-0.031	-0.017	0.353	0.548	0.202	-0.003	-0.035	-0.029	-0.019	-0.012
6	-0.001	-0.015	0.030	-0.018	0.202	0.494	0.202	0.002	-0.057	-0.057	-0.033
7	0.004	-0.017	0.001	-0.058	-0.004	0.269	0.323	0.207	0.037	-0.047	-0.005
8	0.006	-0.011	-0.047	-0.003	-0.047	-0.003	0.207	0.282	0.161	0.044	-0.015

TABLE 10: Model Fit for Path Tangshan-Mashad

Layer	H(km)	Initial Model α(km/sec)	Initial Model β(km/sec)	Initial Model ρ(gr/cm)	Final Model β(km/sec)	SDX_o	SDX
1	10	5.40	2.95	2.80	2.96	0.427	0.059
2	10	6.40	3.15	2.95	3.57	0.427	0.149
3	10	6.45	3.30	3.05	3.60	0.427	0.212
4	10	6.60	3.70	3.12	3.61	0.427	0.280
5	15	7.70	4.55	3.30	4.41	0.349	0.234
6	20	7.50	4.50	3.33	4.35	0.302	0.209
7	25	7.40	4.30	3.35	4.28	0.270	0.201
8	25	7.30	4.20	3.36	4.21	0.270	0.223
9	30	7.30	4.25	3.38	4.24	0.246	0.219
10	30	7.35	4.30	3.39	4.29	0.246	0.235

TABLE 11: Resolution Matrix for Path Tangshan-Mashad

Layer	1	2	3	4	5	6	7	8	9	10
1	0.980	0.039	-0.037	0.016	-0.004	0	-0.001	0	0.001	0
2	0.039	0.877	0.127	-0.063	0.006	0.008	0	-0.007	-0.008	-0.006
3	-0.037	0.128	0.752	0.218	-0.056	-0.030	0.025	0.015	-0.002	-0.009
4	0.016	-0.063	0.218	0.569	0.220	-0.019	-0.054	-0.013	0	-0.001
5	-0.007	0.009	-0.084	0.330	0.546	0.208	-0.008	-0.024	-0.007	-0.009
6	0	0.016	-0.061	-0.038	0.277	0.519	0.253	-0.009	-0.078	-0.059
7	-0.004	0	0.064	0.013	0.014	0.317	0.445	0.251	0.040	-0.053
8	0	-0.019	0.039	-0.033	-0.040	-0.010	0.251	0.317	0.181	0.039

TABLE 12: Model Fit for Path Tangshan-Taipei

		Initial Model		Final Model			
Layer	H(km)	α(km/sec)	β(km/sec)	ρ(gr/cm)	β(gr/cm)	SDX_o	SDX
1	5	4.80	2.90	2.70	2.94	0.185	0.087
2	5	5.25	3.05	2.90	3.01	0.185	0.125
3	10	5.55	3.35	2.96	3.48	0.131	0.073
4	10	6.00	3.70	3.05	3.87	0.131	0.083
5	10	8.10	4.65	3.25	4.46	0.131	0.101
6	15	8.10	4.60	3.30	4.35	0.107	0.091
7	25	8.05	4.45	3.33	4.16	0.083	0.069
8	25	8.00	4.45	3.35	4.27	0.083	0.078
9	25	8.00	4.45	3.36	4.40	0.083	0.081

TABLE 13: Resolution Matrix for Path Tangshan-Taipei

Layer	1	2	3	4	5	6	7	8	9
1	0.779	0.261	-0.025	0.012	0.009	0.002	-0.008	-0.002	0
2	0.261	0.545	0.148	-0.079	-0.015	0.015	0.009	-0.002	-0.003
3	-0.051	0.297	0.686	0.217	-0.053	-0.074	-0.006	-0.006	0.001
4	0.025	-0.158	0.217	0.492	0.246	0.034	-0.056	-0.032	-0.013
5	0.018	-0.031	-0.053	0.246	0.281	0.159	0.001	-0.034	-0.022
6	0.007	0.047	-0.011	0.051	0.239	0.274	0.122	-0.003	-0.030
7	-0.041	0.047	-0.015	-0.014	0.004	0.203	0.295	0.134	0.010

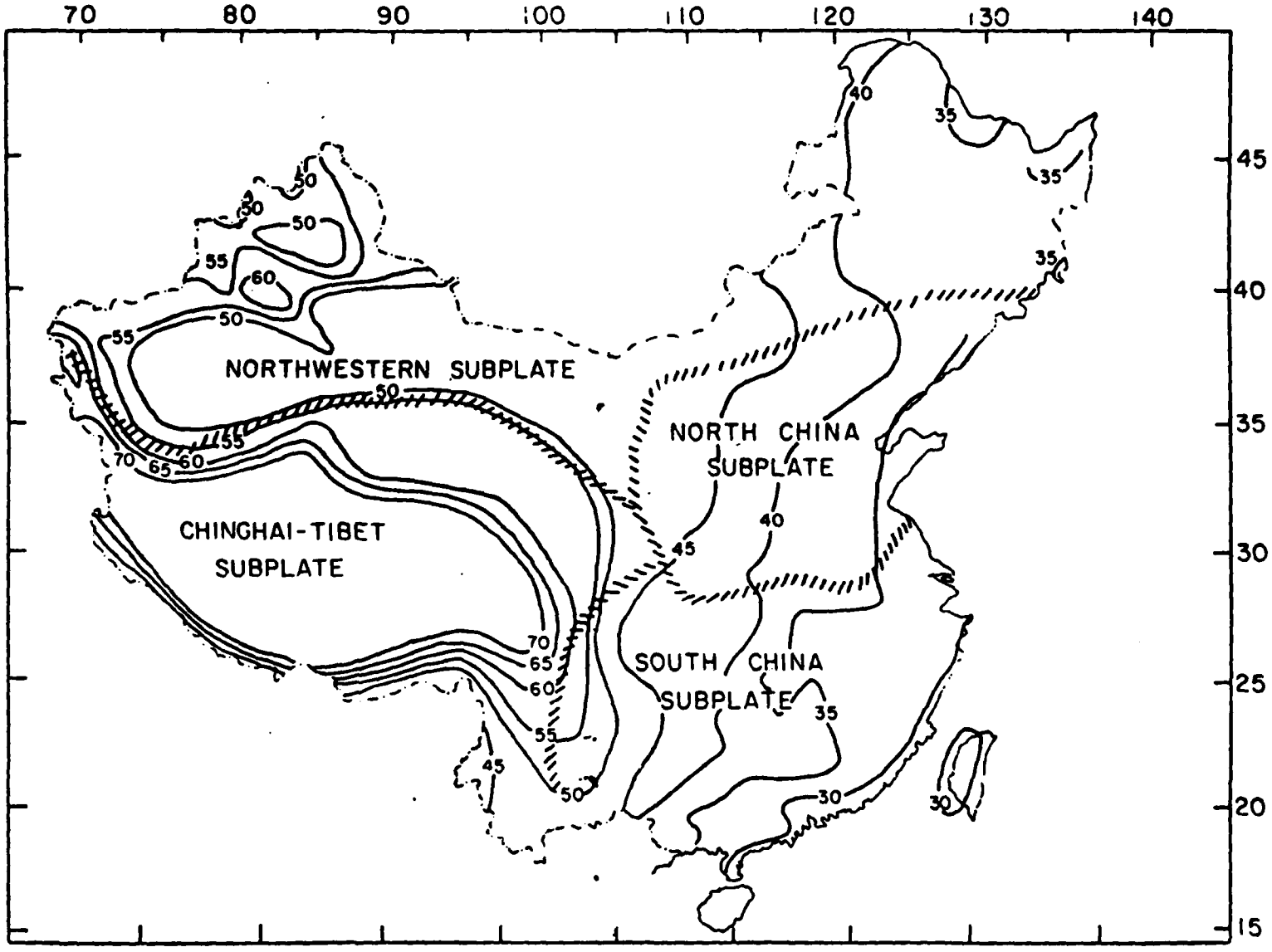

Figure 1. Regional tectonic subdivision of China with inferred crustal thickness shown in 5 km contours (after Chinese Academy of Sciences, 1974).

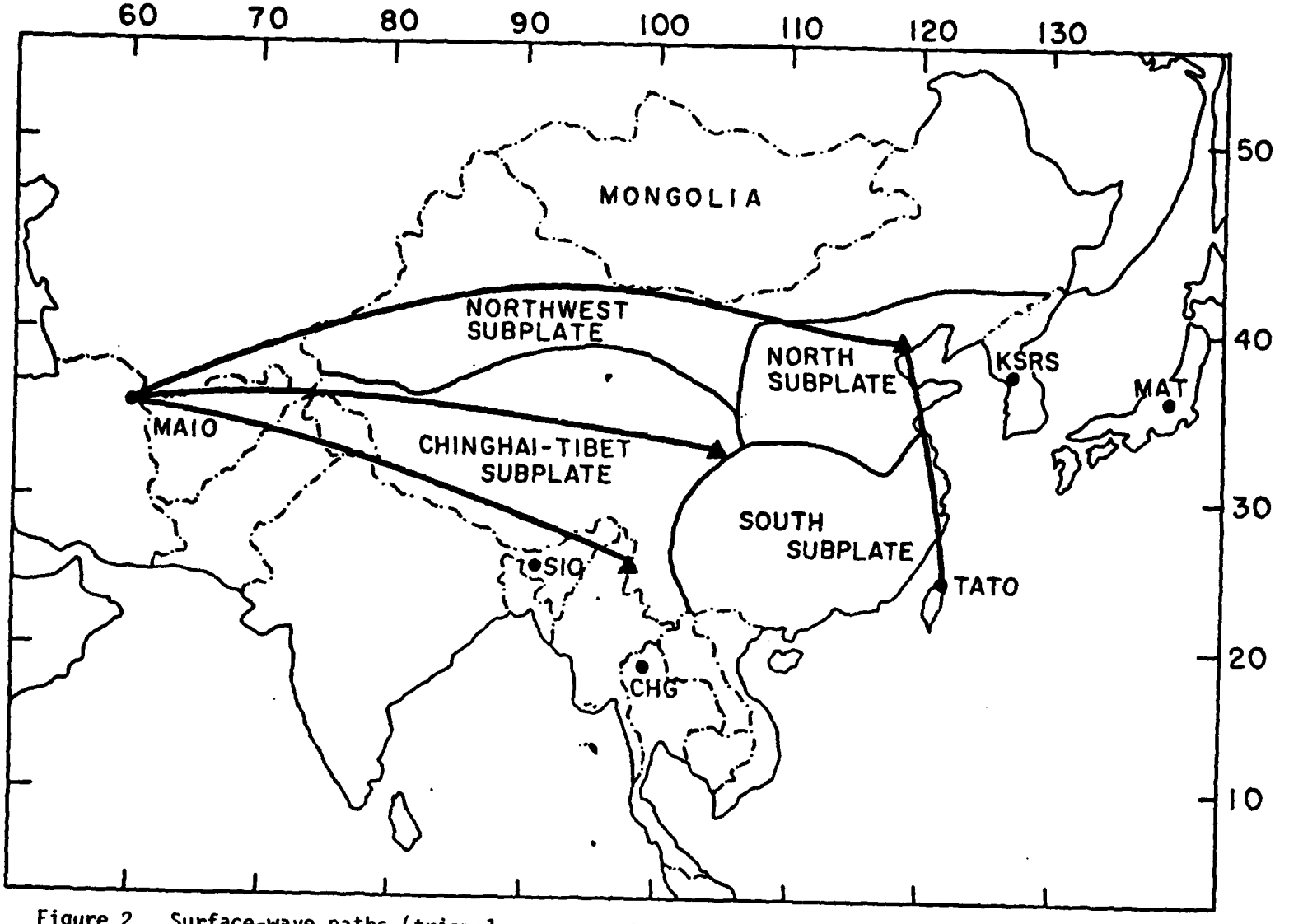

Figure 2. Surface-wave paths (triangles are earthquakes, dots are SRO stations).

Figure 3. Unrotated seismograms for the path Tangshan - Mashad, August 8, 1976 (from top to bottom: vertical, NS, and EW).

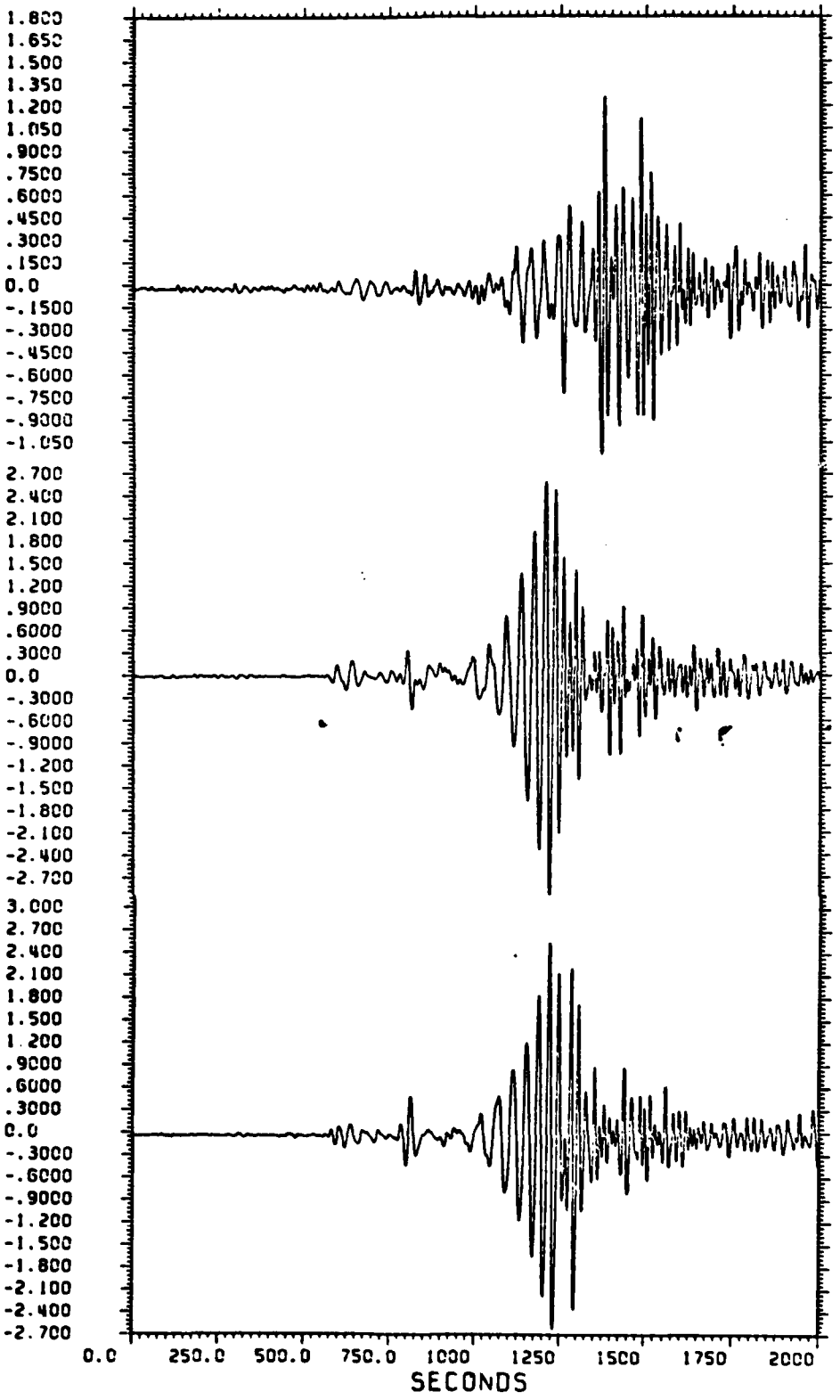

Figure 4. Rotated seismograms for the path Tangshan - Mashad, August 8, 1976 (from top to bottom: vertical, radial, and transverse).

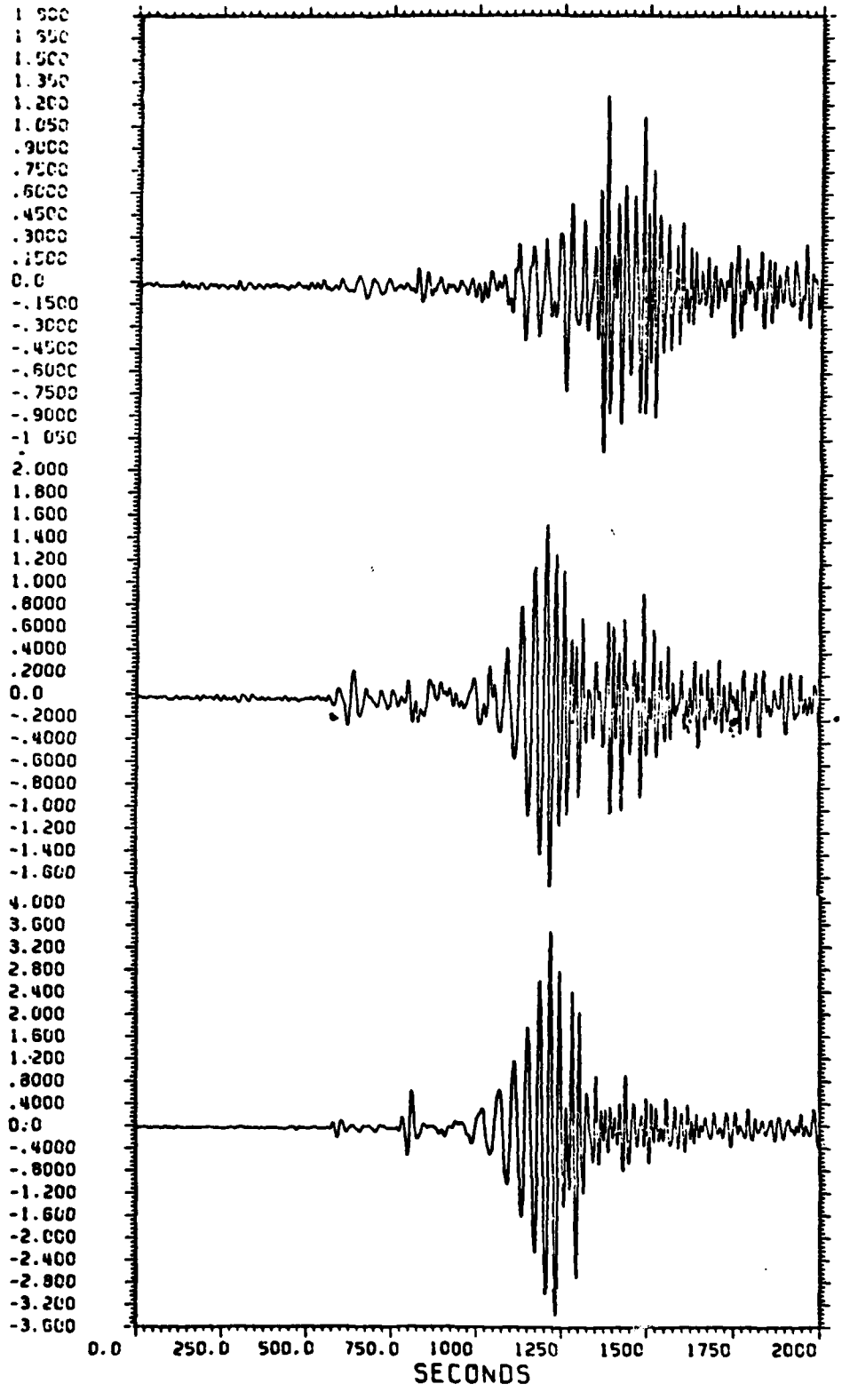

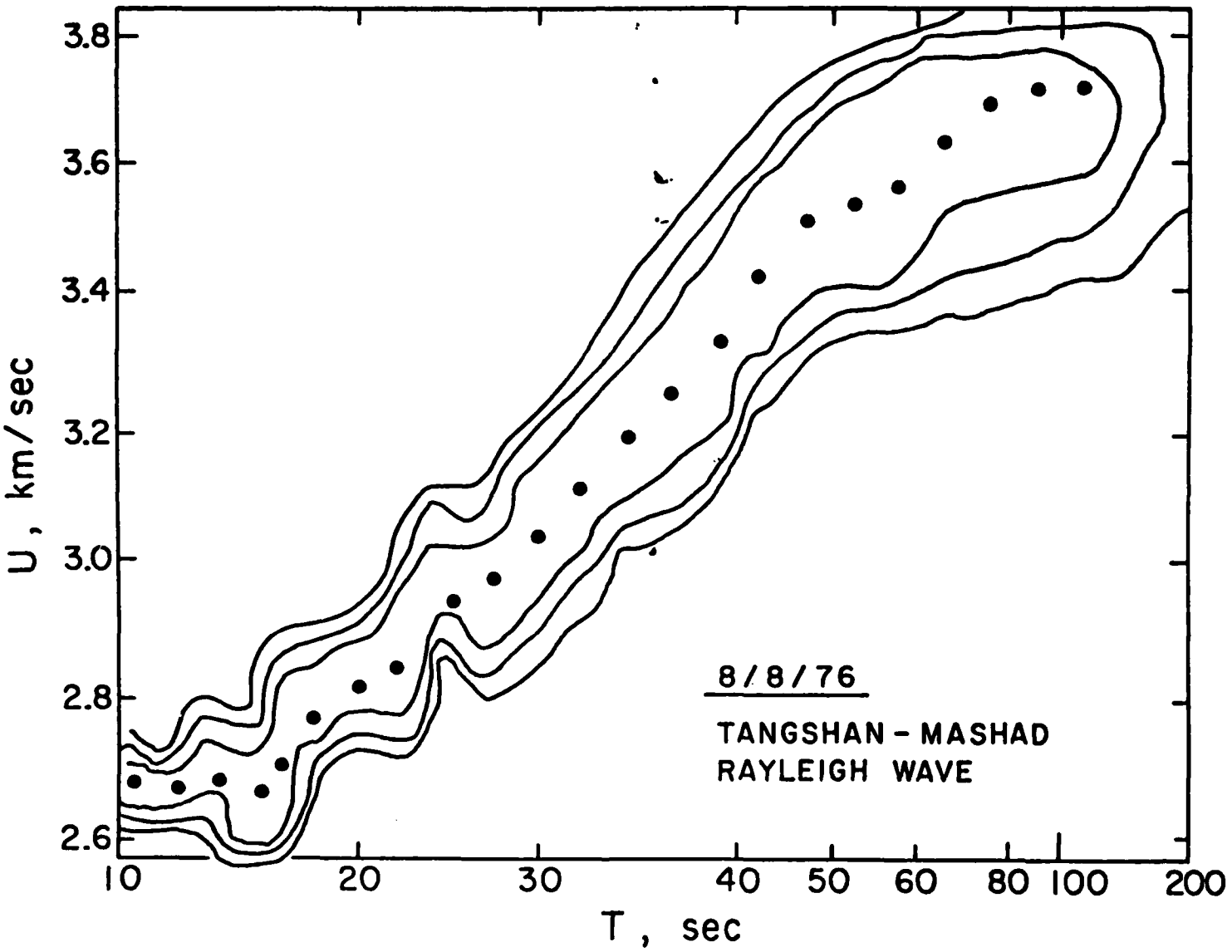

Figure 5. Results of multiple filtering of Rayleigh wave vertical component, Tangshan - Mashad, August 8, 1976.

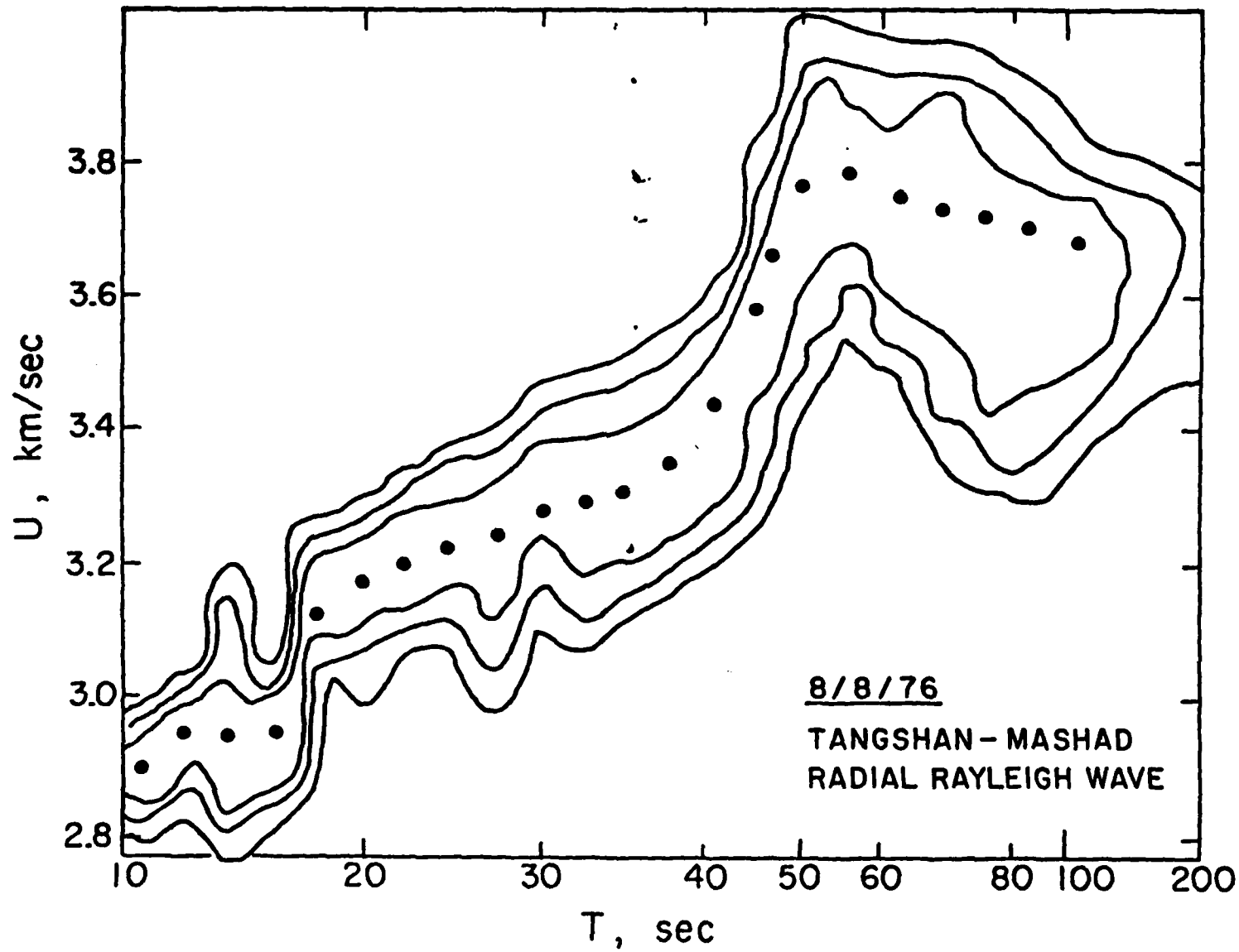

Figure 6. Results of multiple filtering of Rayleigh wave radial component, Tangshan - Mashad, August 8, 1976.

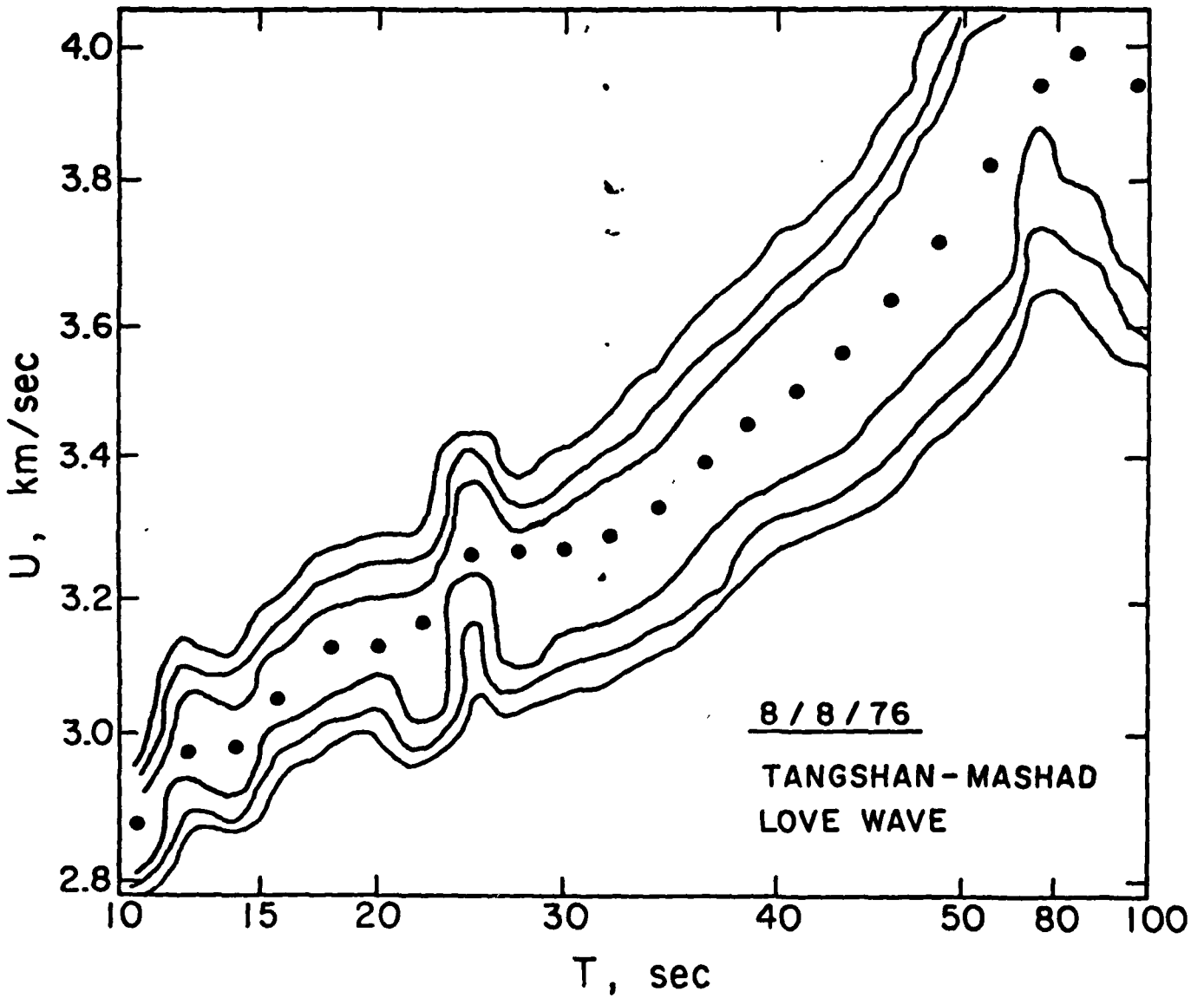

Figure 7. Results of multiple filtering of Love wave, Tangshan - Mashad, August 8, 1976.

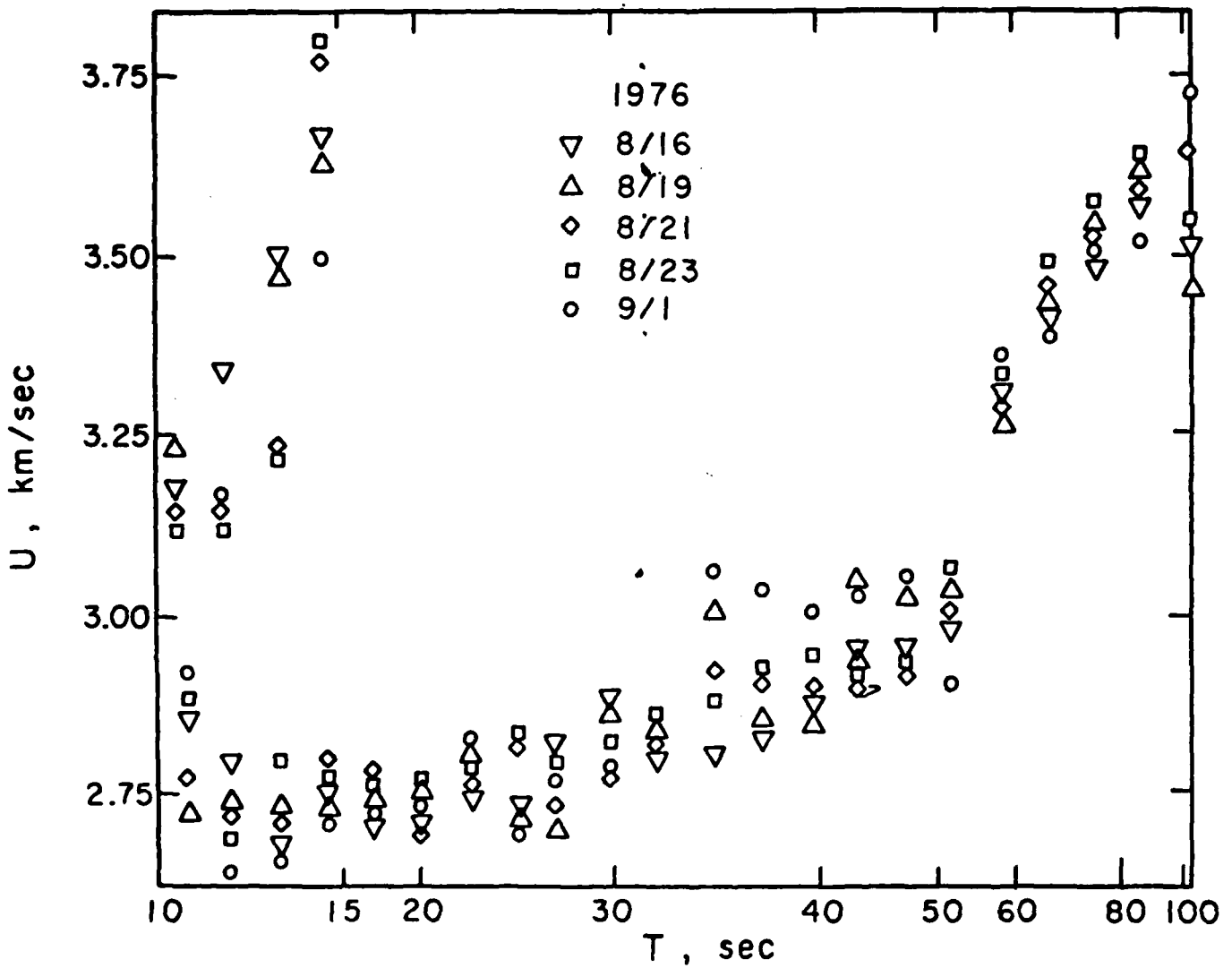

Figure 8. Group velocity of the radial Rayleigh component for five events of the path, Szechwan - Mashad.

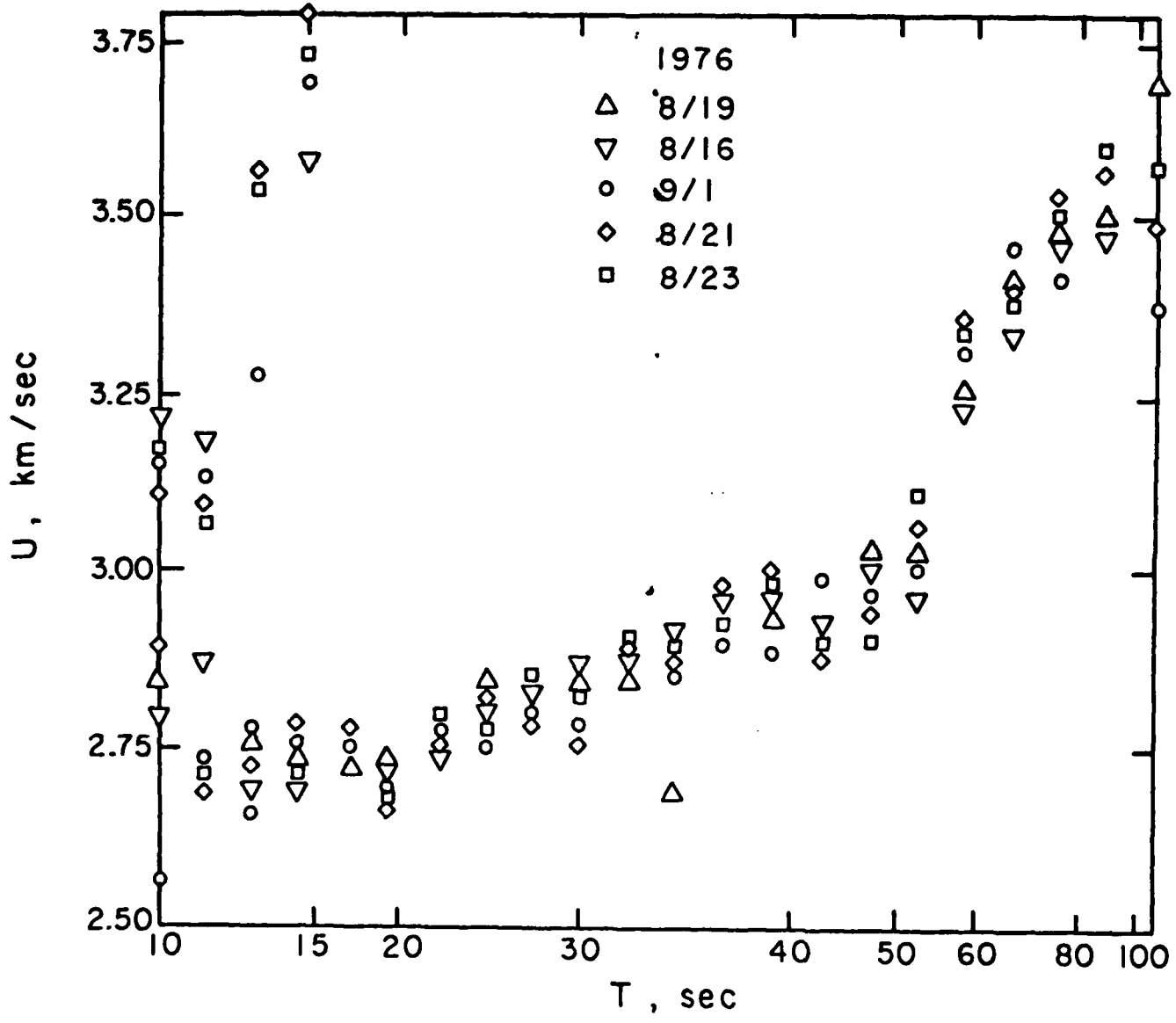

Figure 9. Group velocity of the vertical Rayleigh component for five events of the path Szechwan - Mashad.

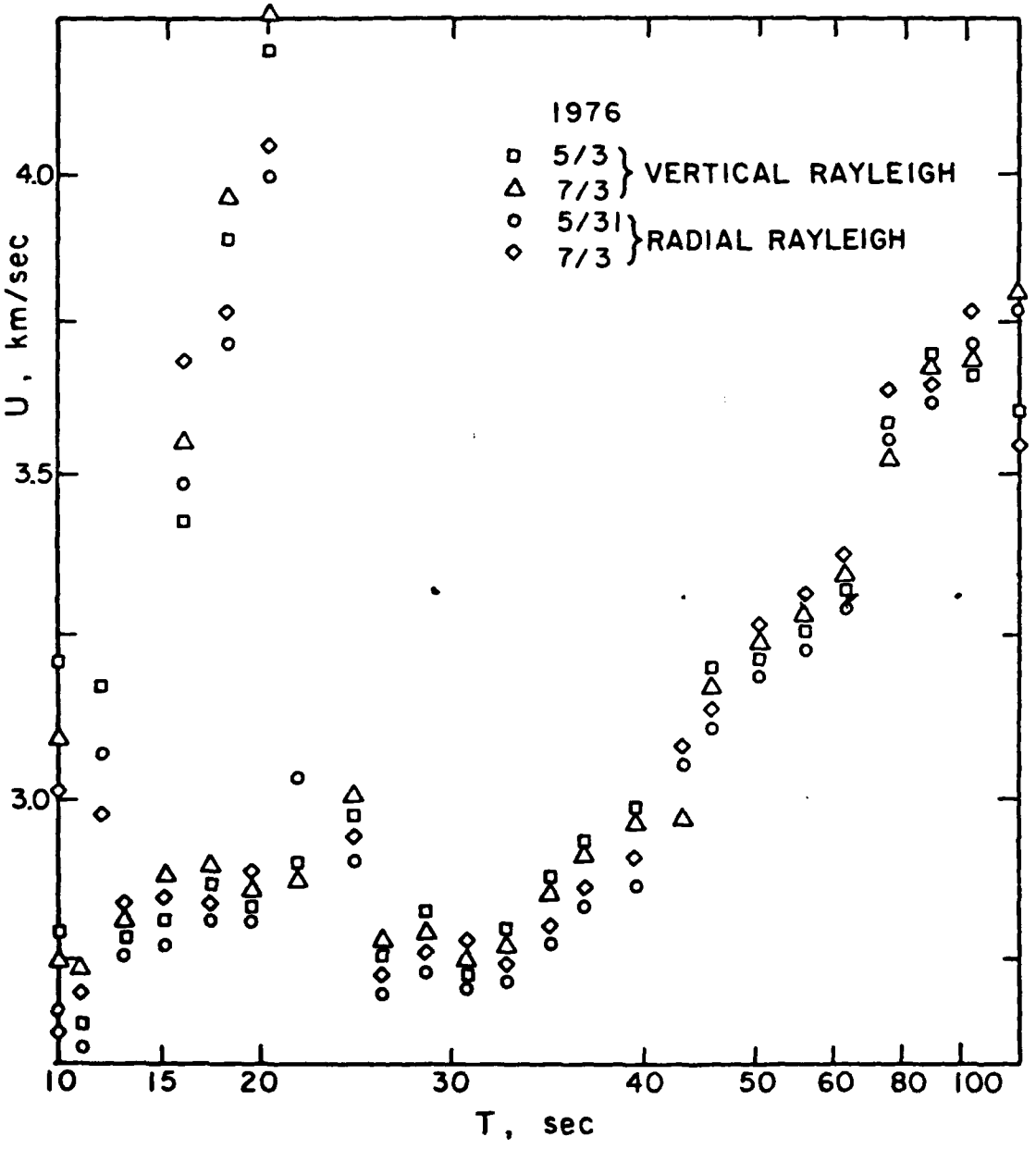

Figure 10. Rayleigh wave group velocity for three events of the path, Yunan - Mashad.

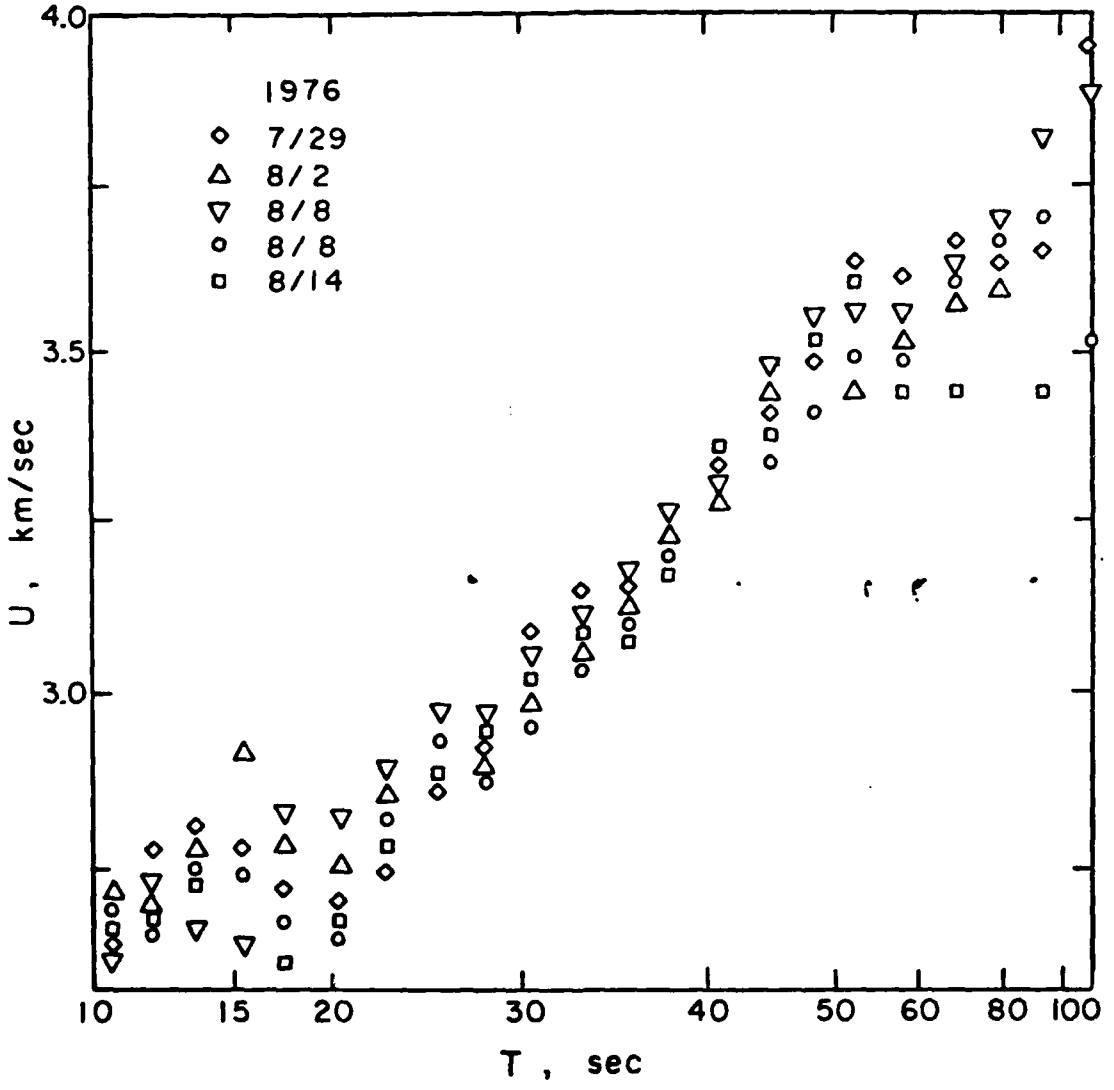

Figure 11. Group velocity of Rayleigh waves for five events of the path, Tangshan - Mashad.

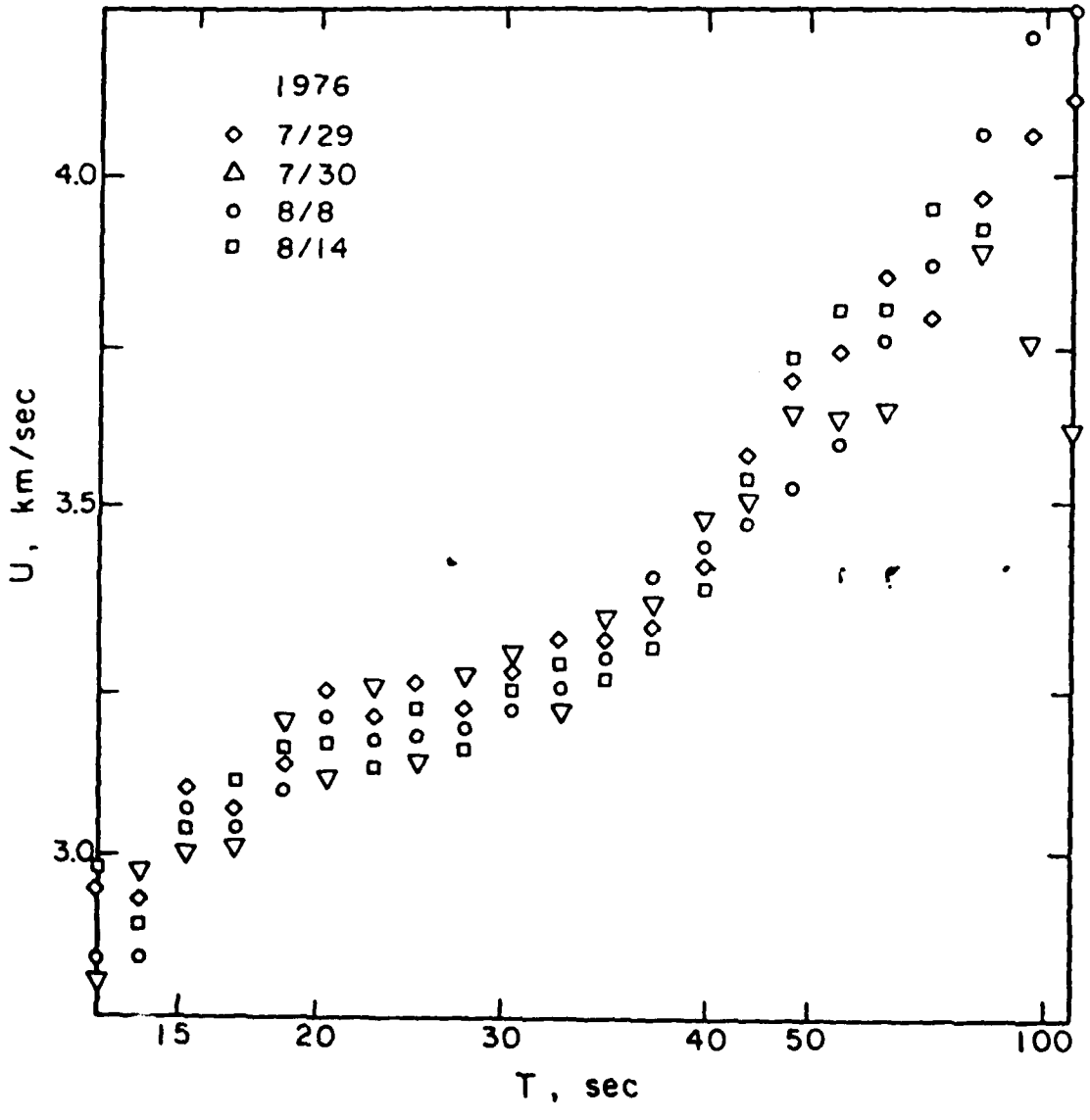

Figure 12. Love wave group velocity for four events of the path, Tangshan - Mashad.

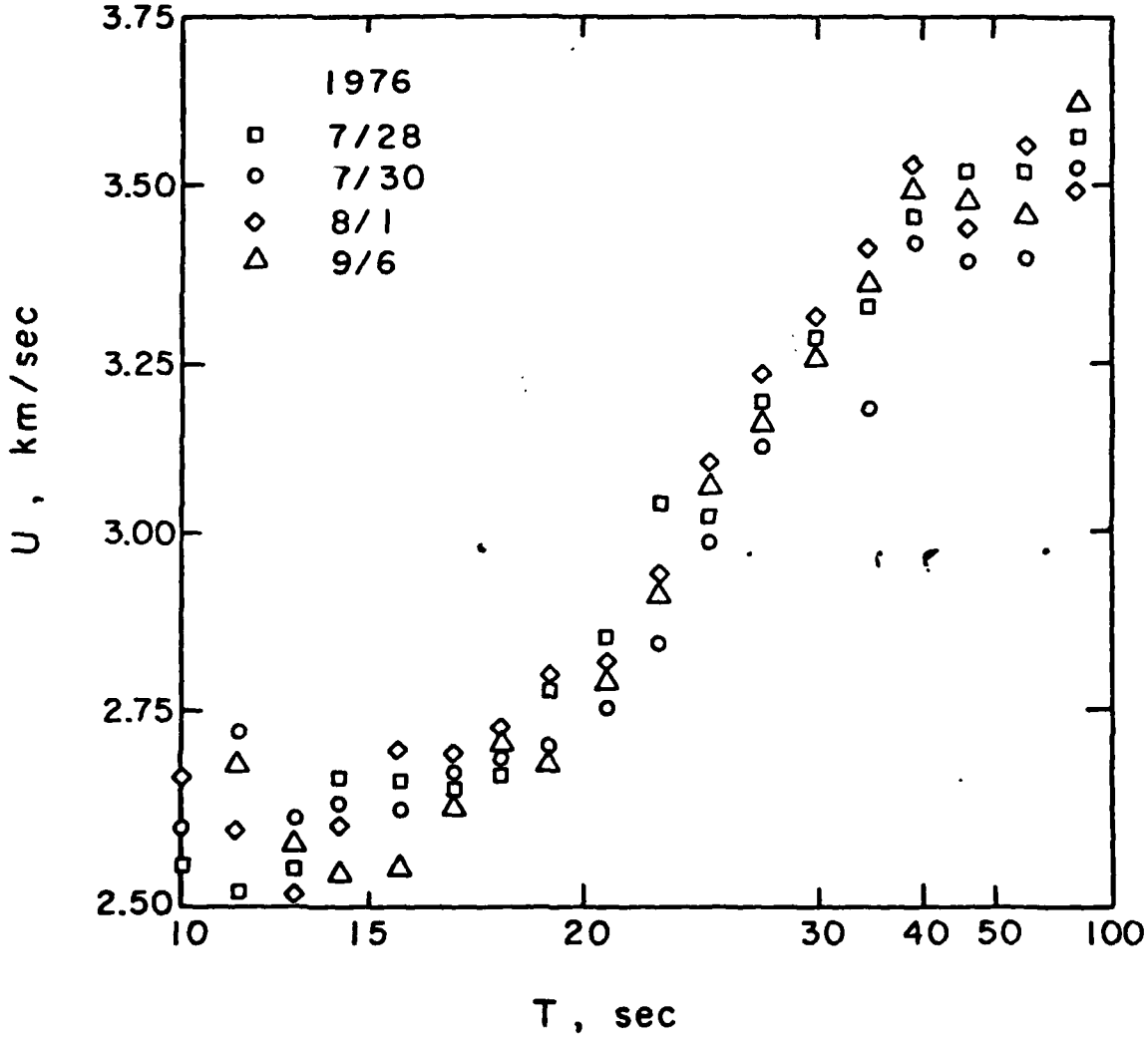

Figure 13. Vertical component Rayleigh wave group velocity for four events of the path, Tangshan - Taipei.

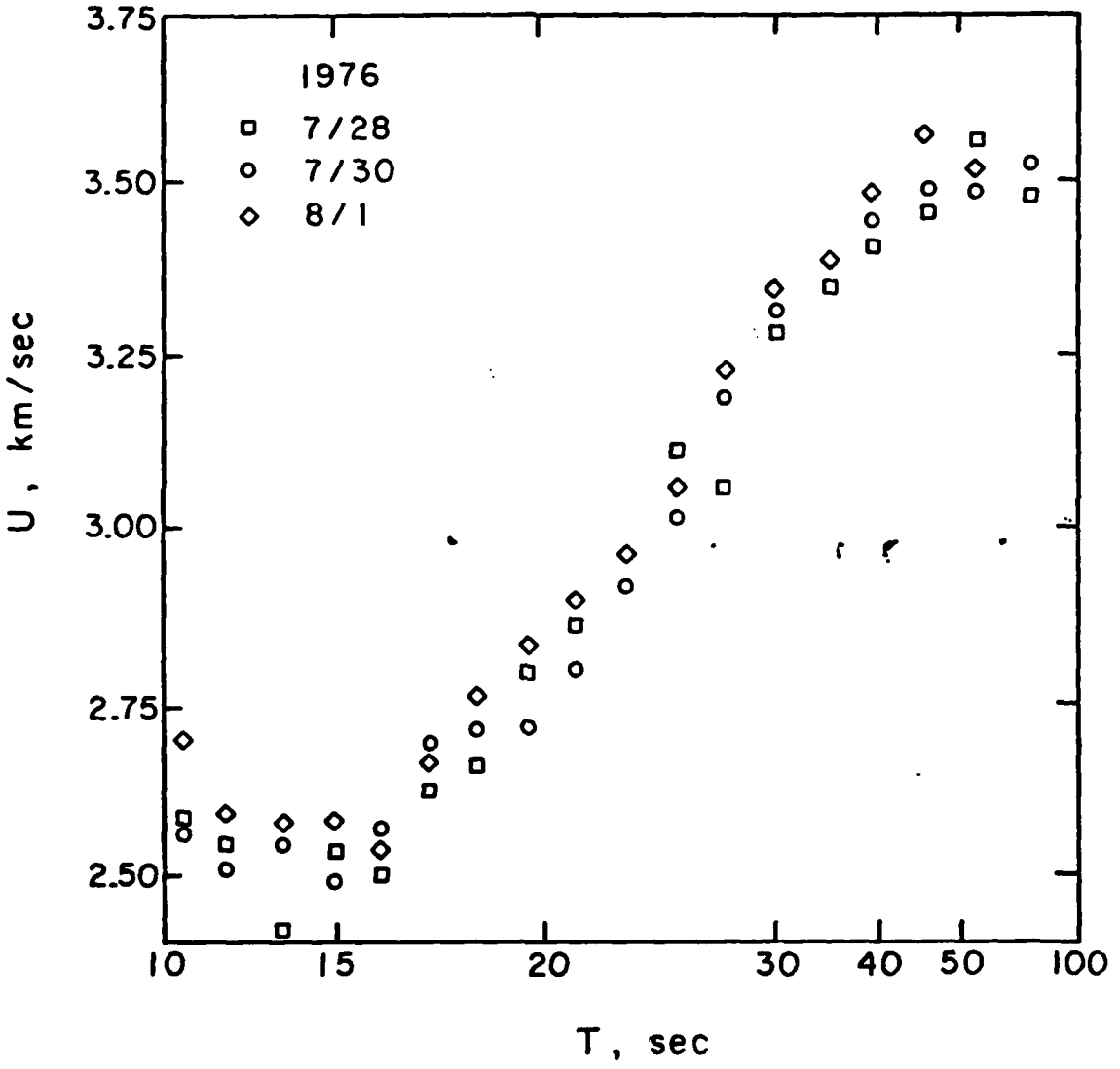

Figure 14. Radial component Rayleigh wave group velocity for three events of the path, Tangshan - Taipei.

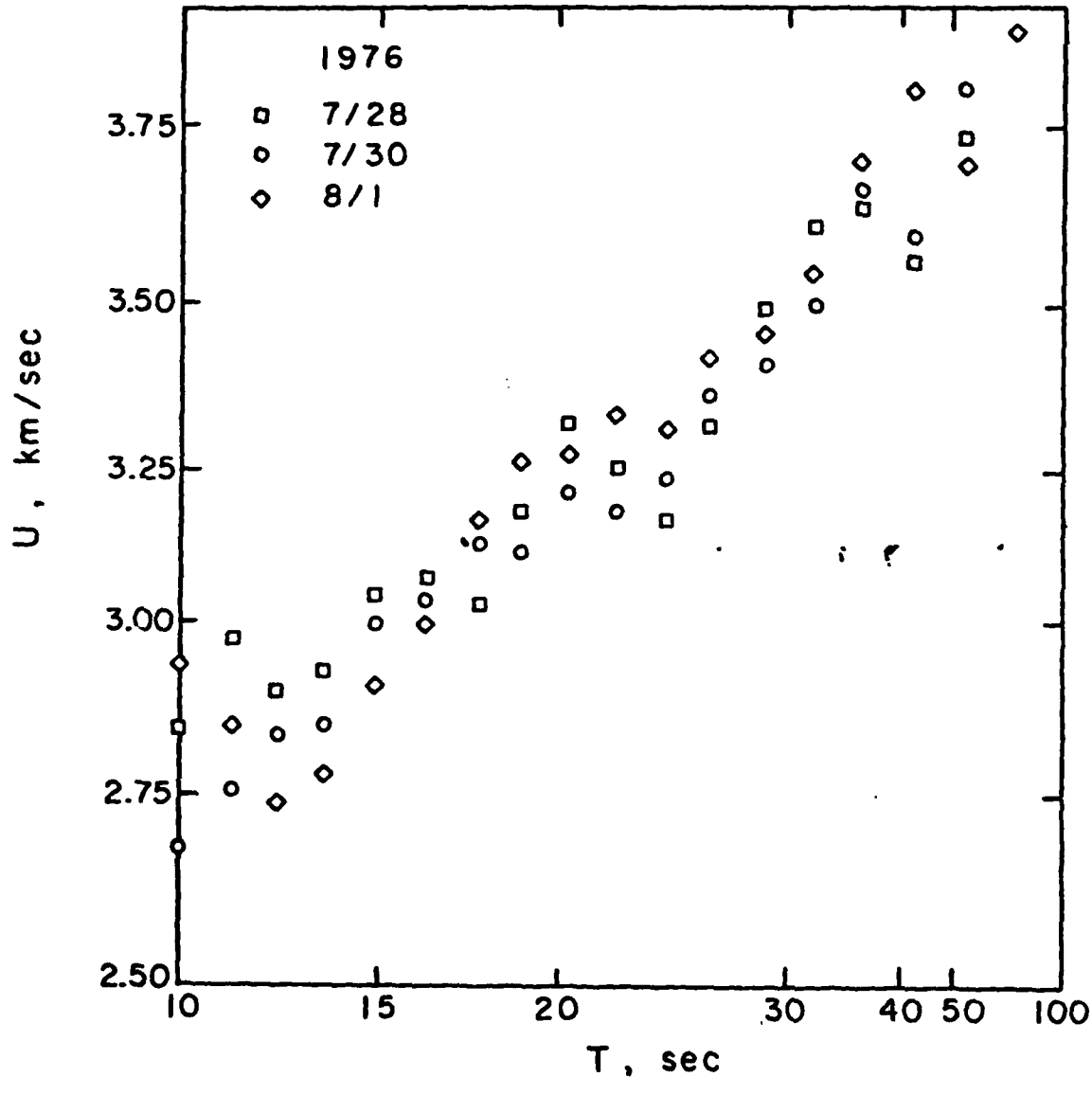

Figure 15. Love wave group velocity for three events of the path, Tangshan - Taipei.

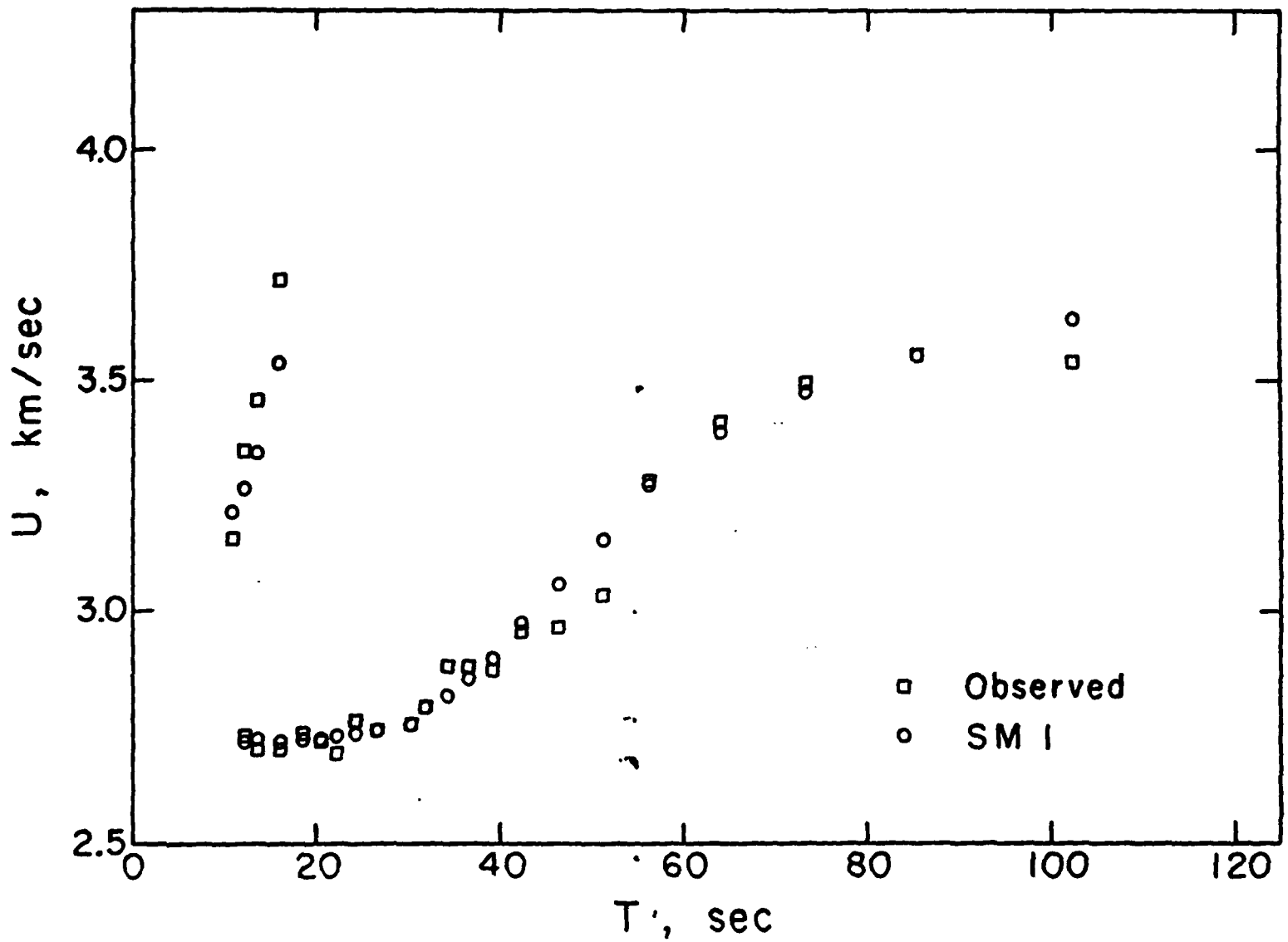

Figure 16. Theoretical and observed group velocities for the path, Szechwan - Mashad.

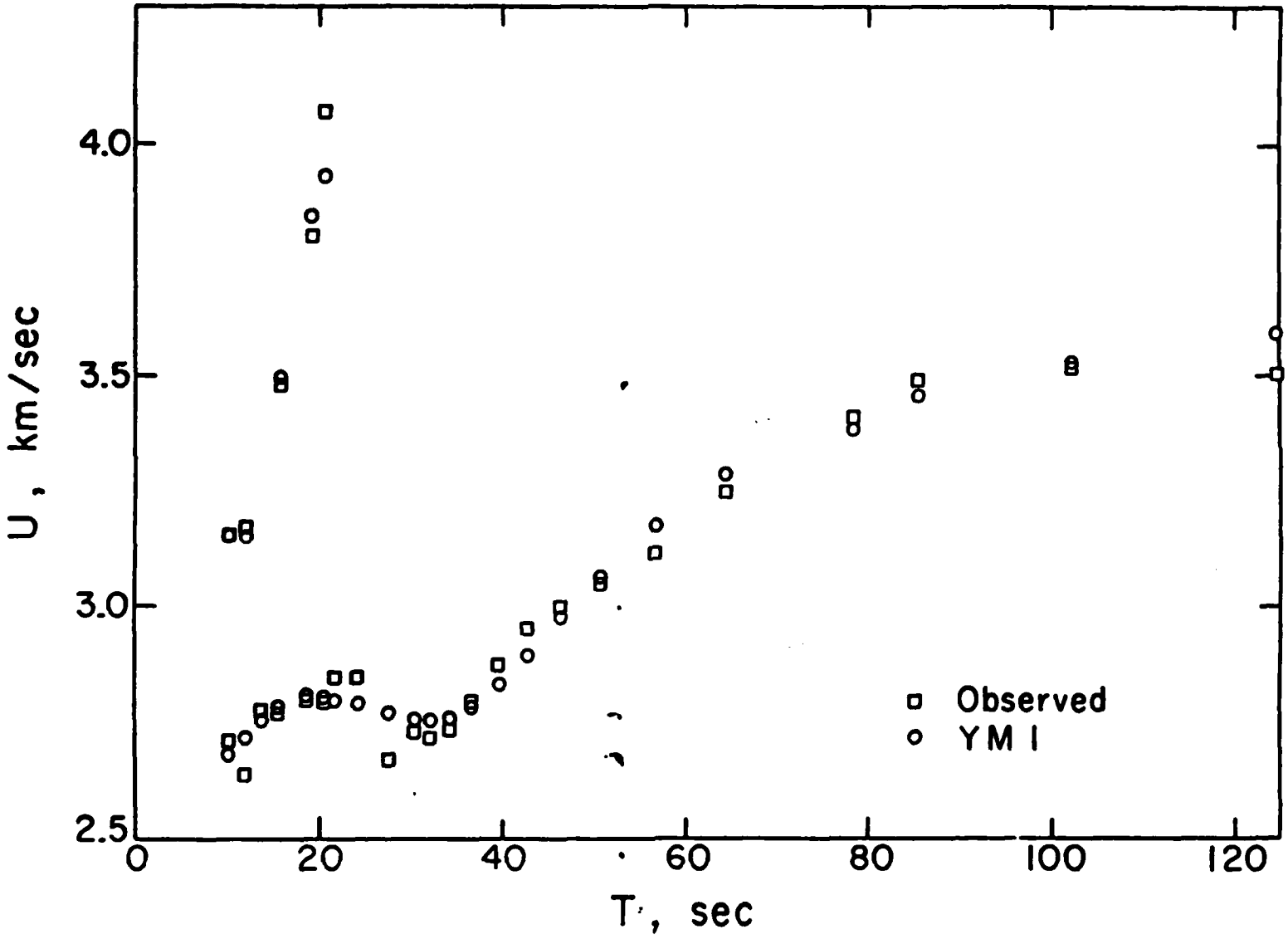

Figure 17. Theoretical and observed group velocities for the path Yunan-Mashad.

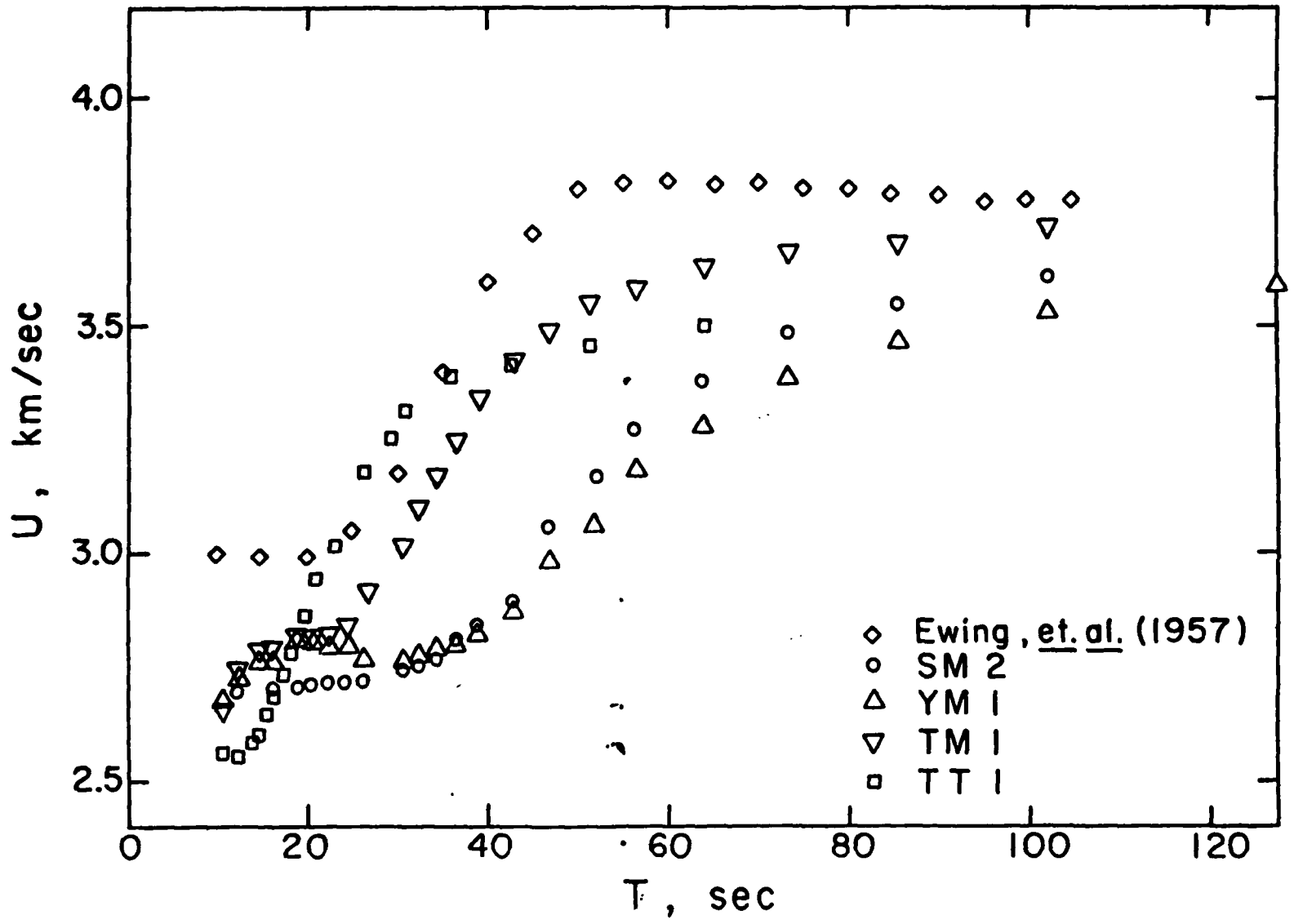

Figure 18. Comparison of Rayleigh wave group velocities for several paths across China with average continental dispersion (Ewing et al., 1957).

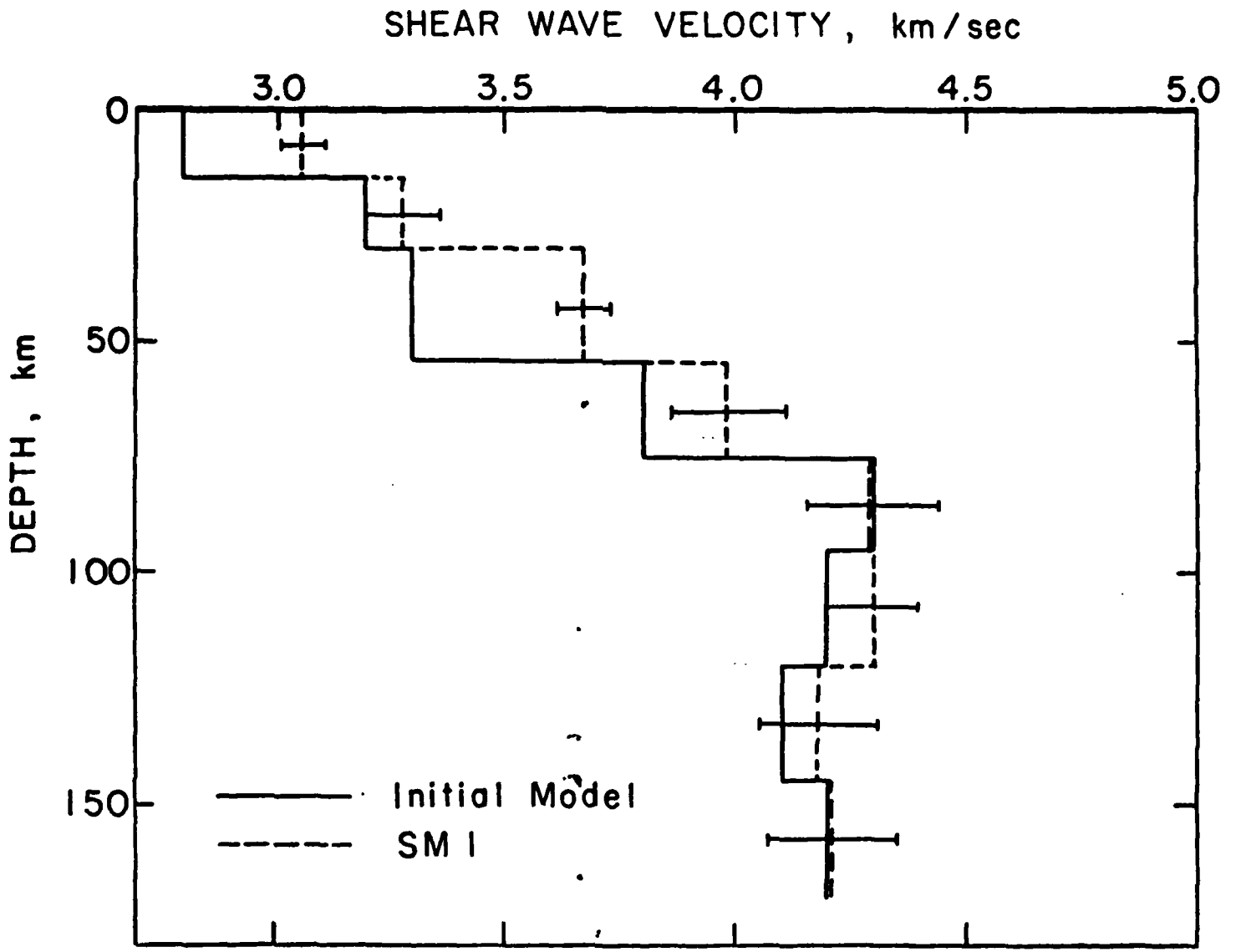

Figure 19. Resulting shear wave velocity model for the parth Szechwan-Mashad.

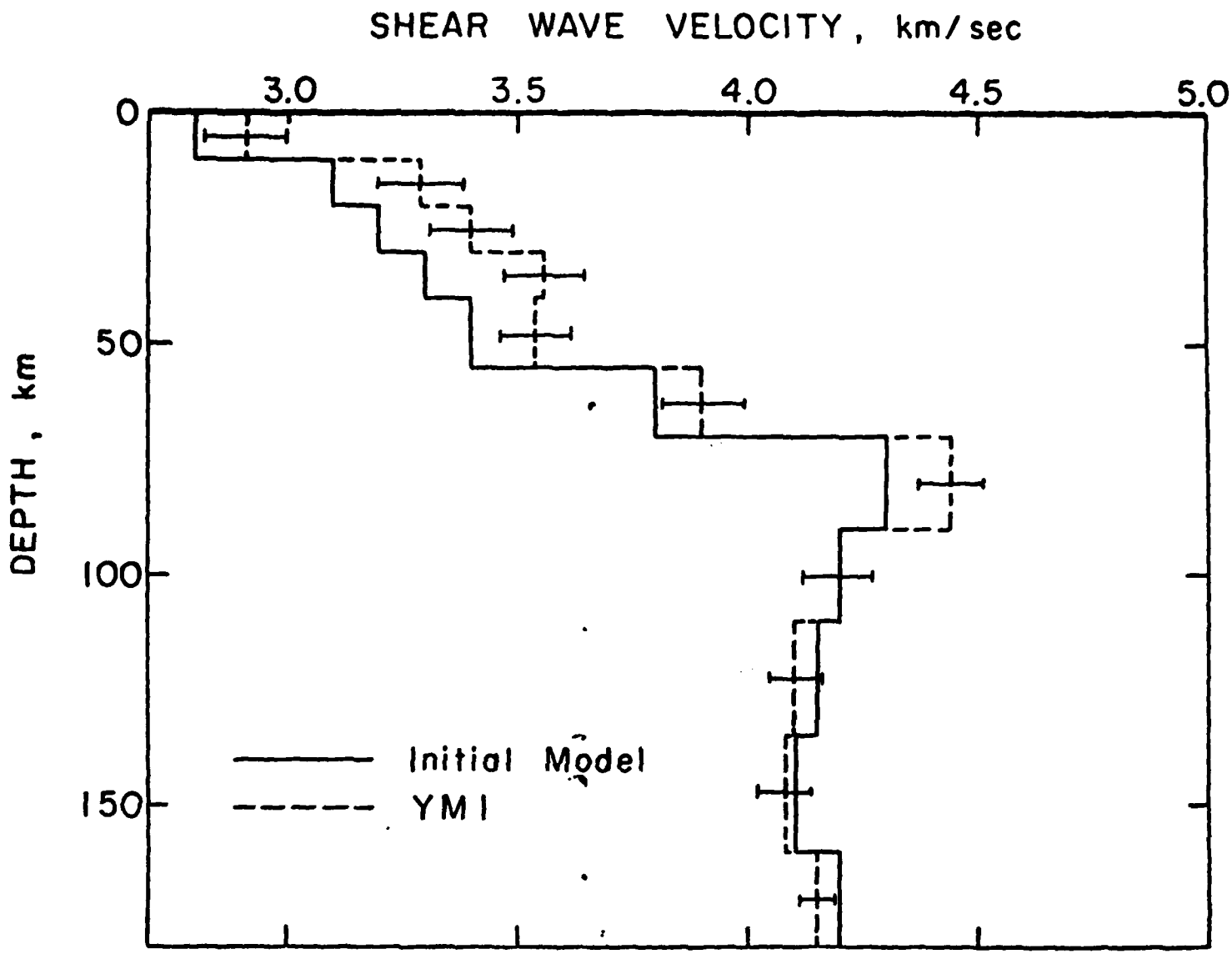

Figure 20. Resulting shear wave velocity model for the path Yunan-Mashad.

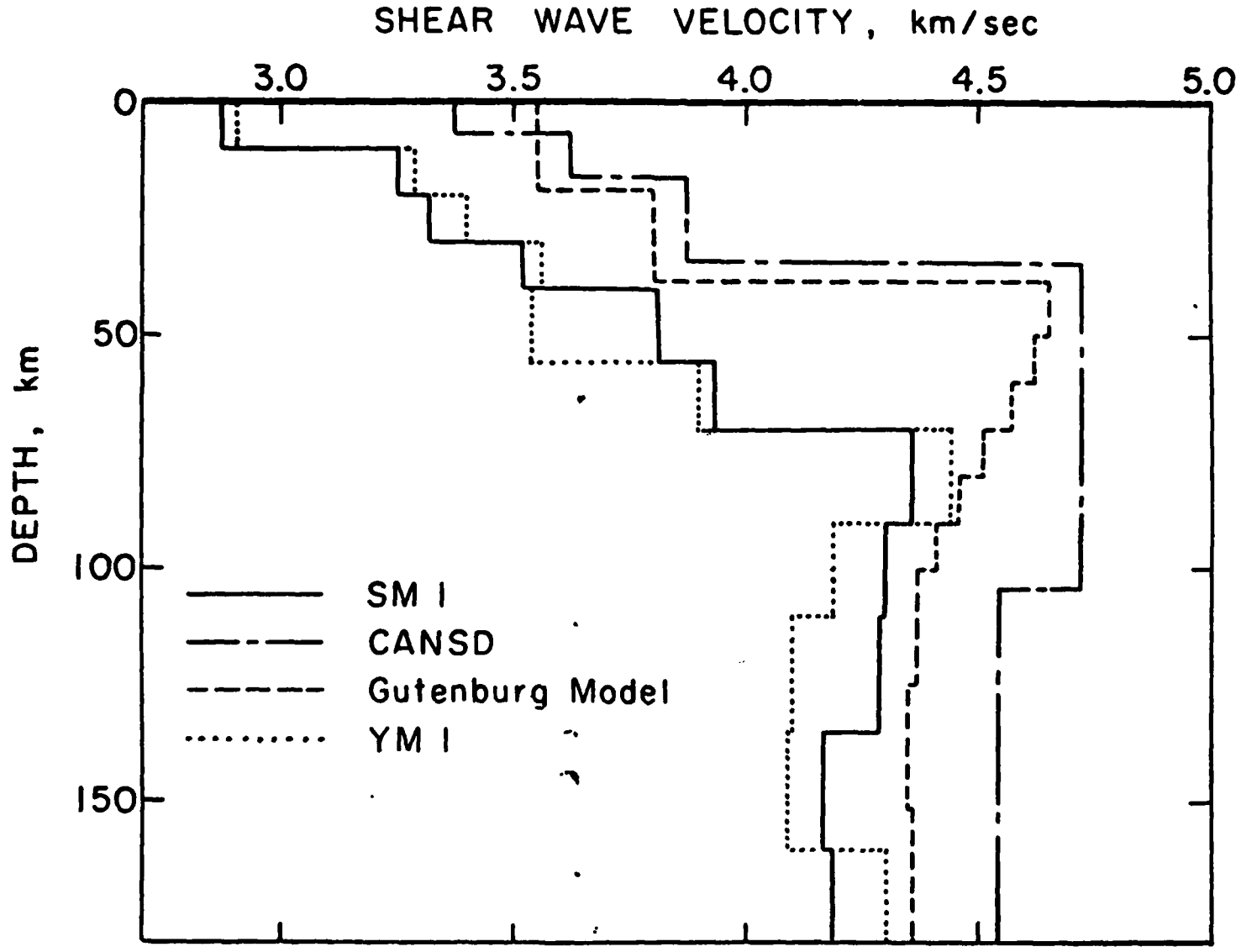

Figure 21. Comparison of the Canadian Shield model (Brune and Dorman, 1963) and the Gutenberg model (Takeuchi et al., 1964) with model SM1 and YM1.

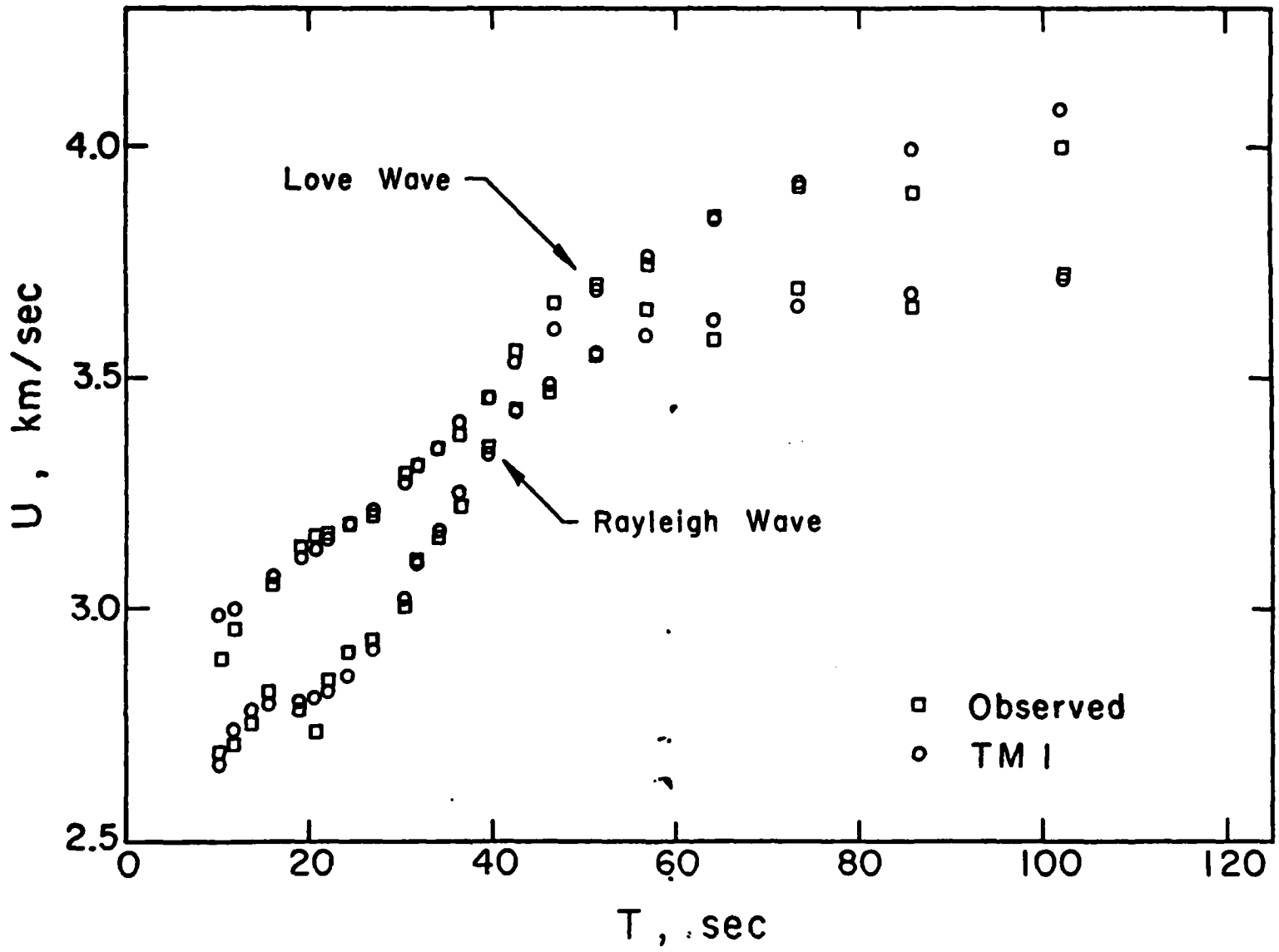

Figure 22. Theoretical and observed group velocities for the Tangshan-Mashad path.

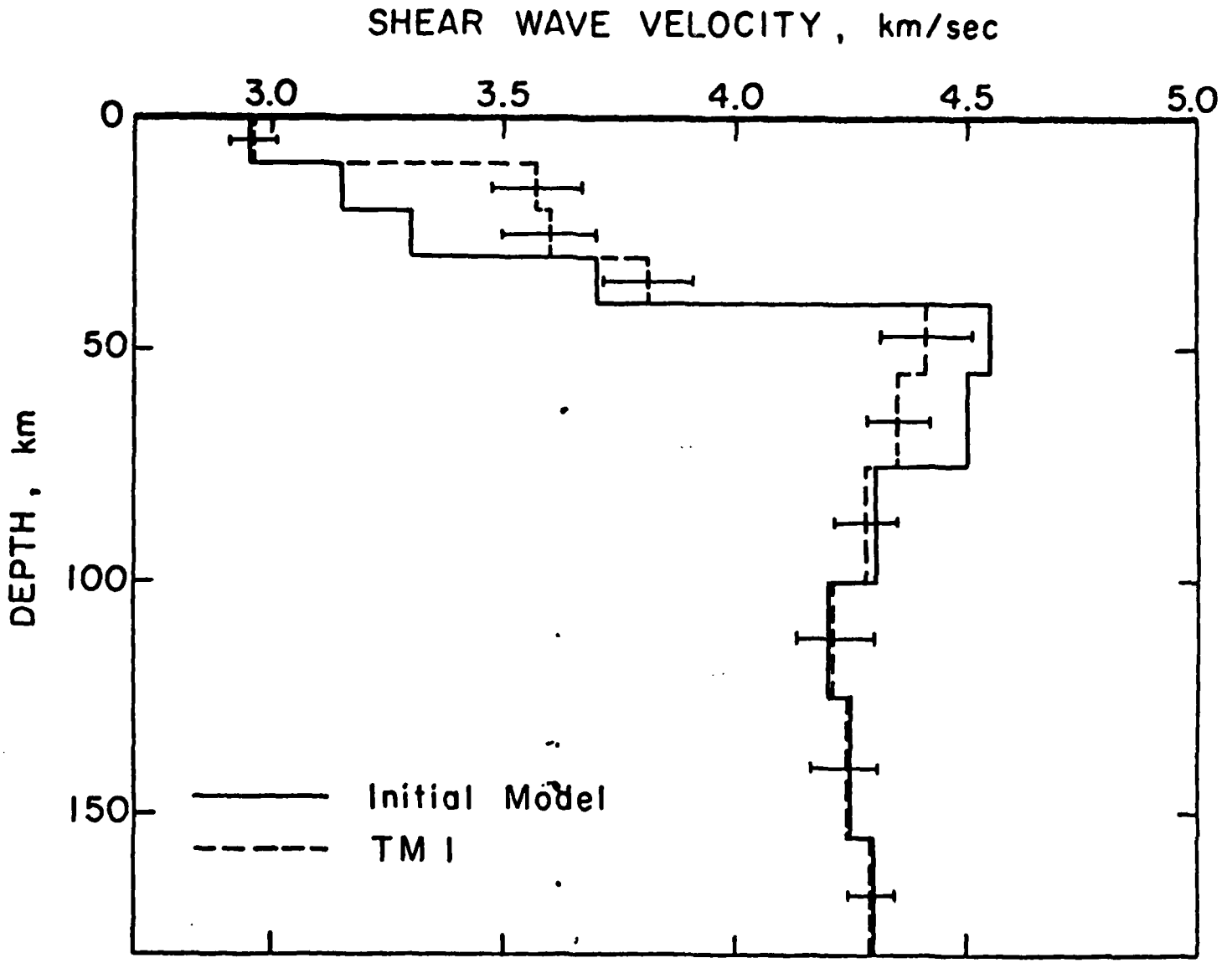

Figure 23. Resulting shear wave velocity model for the Tangshan-Mashad path.

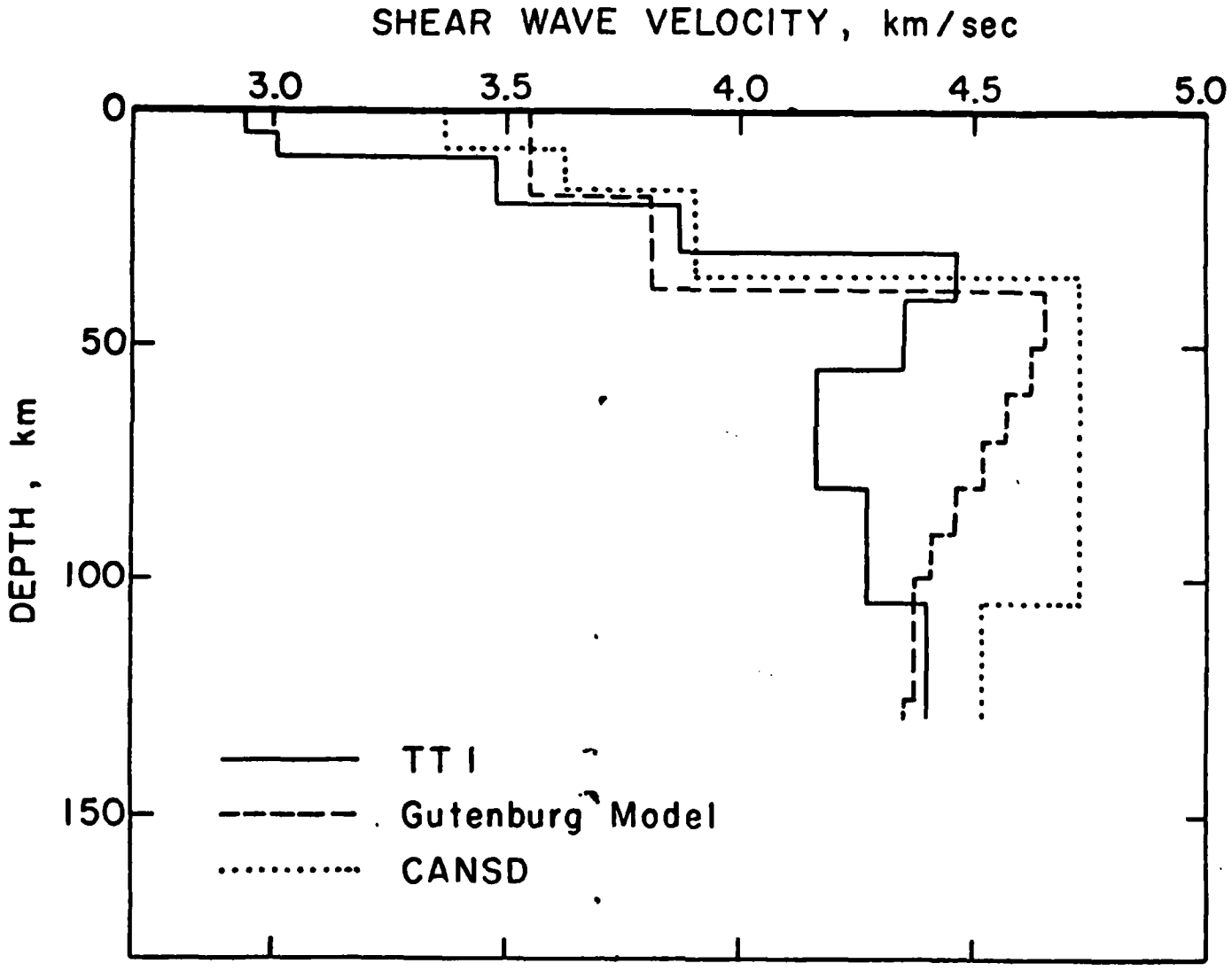

Figure 24. Comparison of the Canadian Shield Model (Brune and Dorman, 1963) and the Gutenberg Model (Takeuchi et al., 1964) with model TM1.

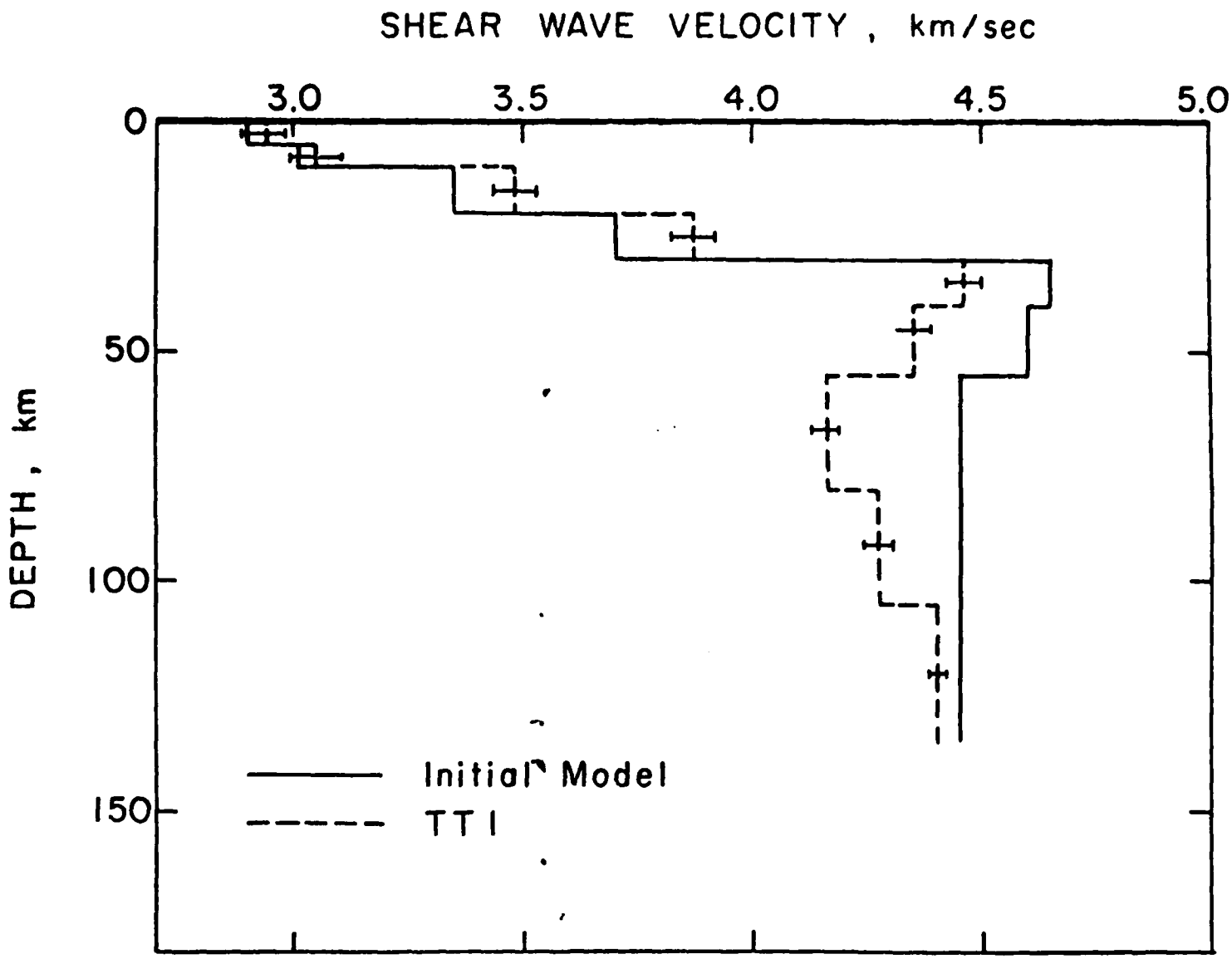

Figure 26. Resulting shear wave velocity for the path Tangshan-Taipei.

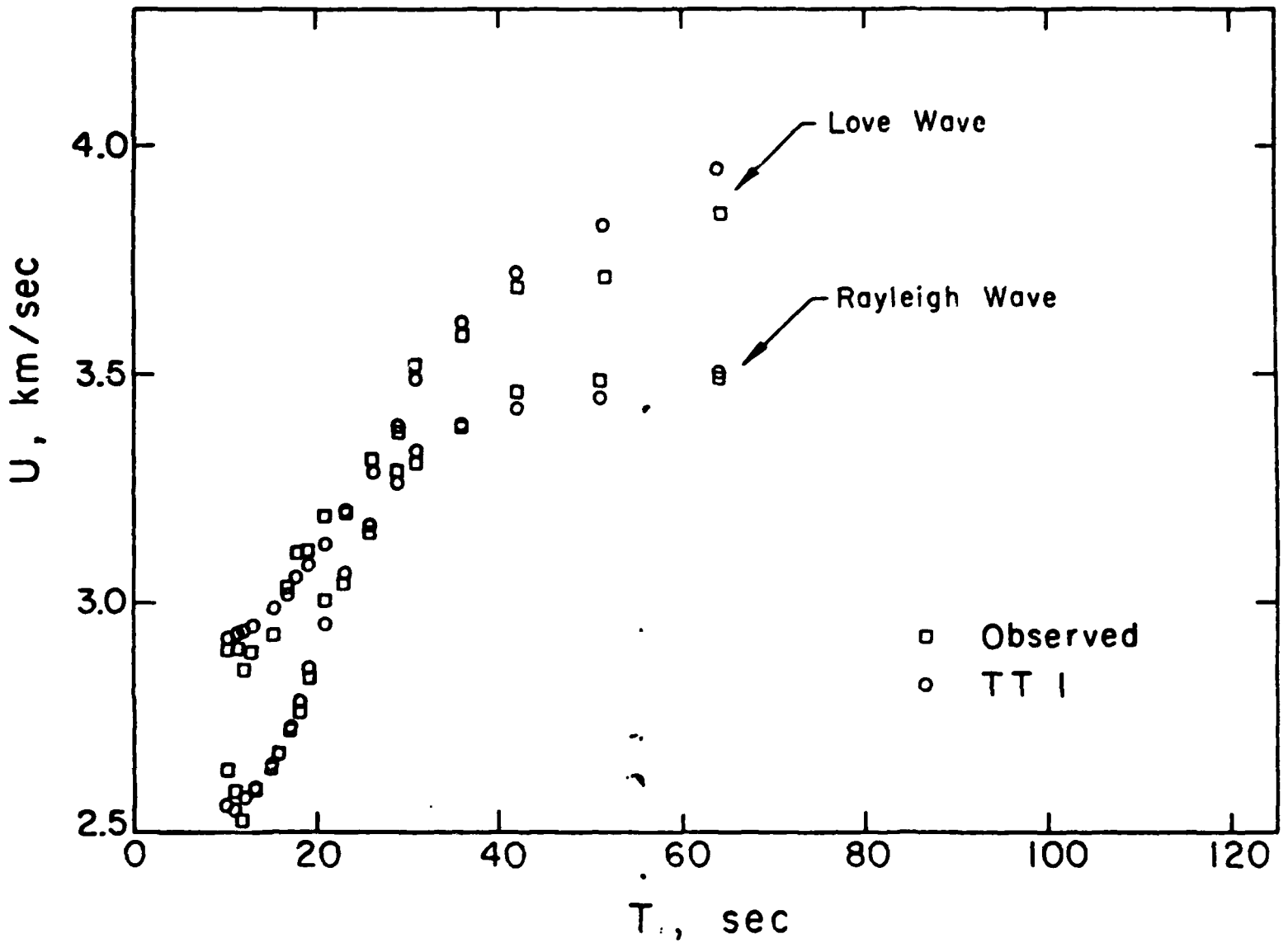

Figure 25. Observed and theoretical group velocities for the path Tangshan-Taipei.

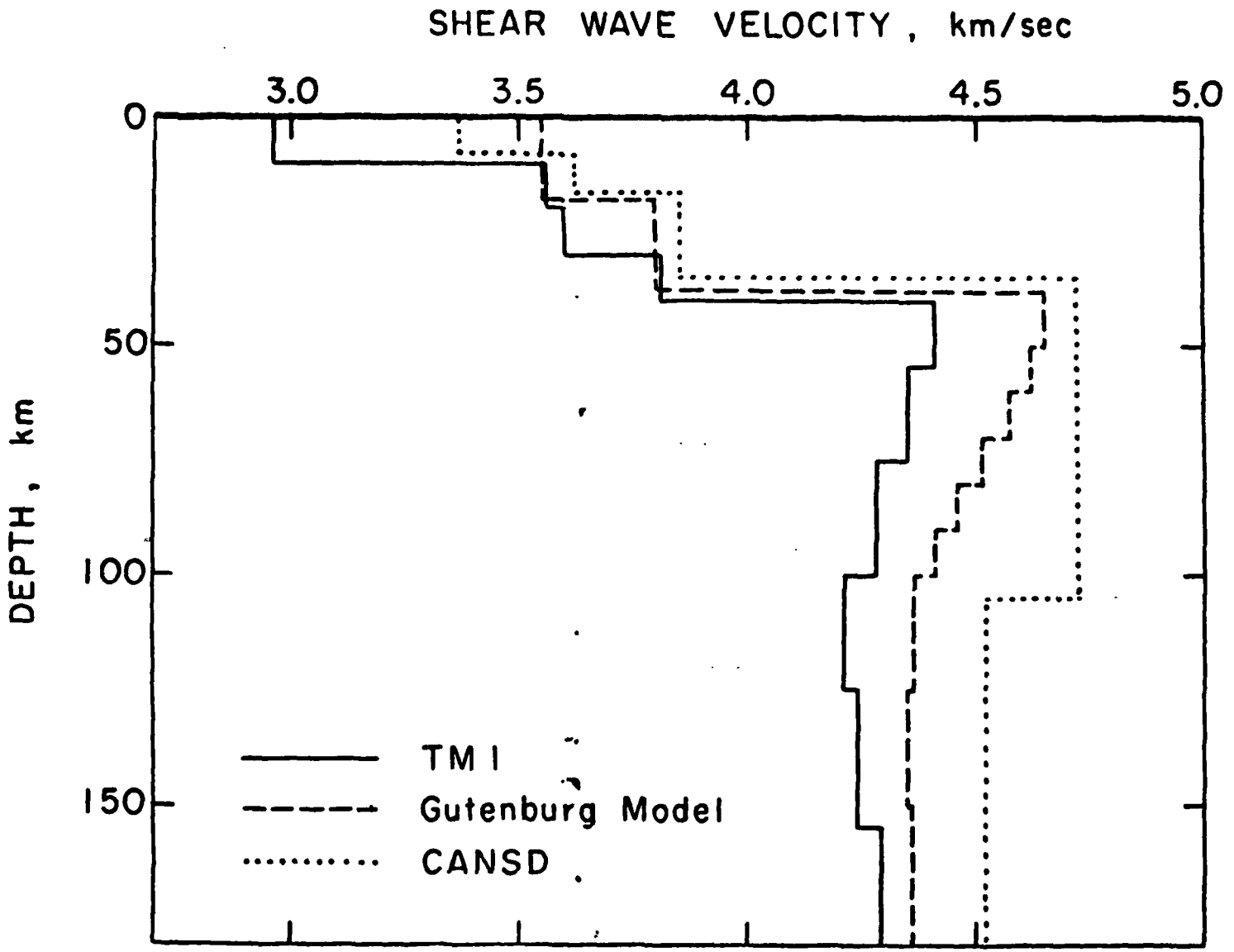

Figure 27. Comparison of Canadian Shield Model (Brune and Dorman, 1963) and the Gutenberg Model (Takeuchi et al., 1964) with model TTI.